Molecular Neurobiology (2019) 56:6833–6855
https://doi.org/10.1007/s12035-019-1551-0

Prominent Postsynaptic and Dendritic Exocytosis of *Endogenous* BDNF Vesicles in BDNF-GFP Knock-in Mice

Julia Leschik[2] · Robert Eckenstaler[1] · Thomas Endres[1] · Thomas Munsch[1,6] · Elke Edelmann[1,6] · Karin Richter[4] · Oliver Kobler[3] · Klaus-Dieter Fischer[4] · Werner Zuschratter[3] · Tanja Brigadski[1,7] · Beat Lutz[2,5] · Volkmar Lessmann[1,6]

Received: 21 December 2018 / Accepted: 13 March 2019 / Published online: 30 March 2019

Abstract

Brain-derived neurotrophic factor (BDNF) is a secreted messenger molecule that is crucial for neuronal function and induction of synaptic plasticity. Although altered availability of BDNF underlies many neurological deficits and neurodegenerative disorders, secretion dynamics of *endogenous* BDNF are unexplored. We generated a BDNF-GFP knock-in (KiBE) mouse, in which GFP-labeled BDNF is expressed under the control of the unaltered endogenous mouse BDNF gene regulatory elements. This KiBE mouse model enables for the first time live cell imaging analysis of *endogenous* BDNF dynamics. We show that BDNF-GFP release and biological activity in vivo are unaffected by the GFP tag, since homozygous KiBE mice, which lack wild-type BDNF, are healthy and have a normal life expectancy. STED superresolution microscopy shows that 70% of BDNF-GFP vesicles in KiBE mouse neurites are localized in dendrites, being typically 200 nm away from synaptic release sites. Live cell imaging in hippocampal slices also reveals prominent targeting of *endogenous* BDNF-GFP vesicles to dendrites. Fusion pore opening and cargo release of dendritic BDNF vesicles start within 30 s after a strong depolarizing stimulus and continue for > 100 s thereafter, revealing an astonishingly delayed and prolonged release of *endogenous* BDNF.

Keywords Neurotrophin · BDNF · Neuropeptide secretion · Hippocampus · Exocytosis · Secretory granules · GFP knock-in

Introduction

The neurotrophin brain-derived neurotrophic factor (BDNF) regulates survival and differentiation during neural development and is crucially involved in synaptic plasticity, learning, and memory formation in the adult brain [1–5]. In the brain, BDNF expression is observed exclusively in glutamatergic neurons, while it is absent from inhibitory neurons. With few exceptions, BDNF is expressed at extraordinarily low levels, ensuring its strong command for regulation once a small amount is locally released. Due to its low abundance, dynamics of targeting and release of *endogenous* BDNF

Julia Leschik and Robert Eckenstaler both share equal contribution as first authors.

Beat Lutz and Volkmar Lessmann both shared senior authorship.

Electronic supplementary material The online version of this article (https://doi.org/10.1007/s12035-019-1551-0) contains supplementary material, which is available to authorized users.

✉ Volkmar Lessmann
lessmann@med.ovgu.de

[1] Institute of Physiology, Medical Faculty, Otto-von-Guericke University, Leipziger Str. 44, D-39120 Magdeburg, Germany

[2] Institute of Physiological Chemistry, University Medical Center of the Johannes Gutenberg University, D-55128 Mainz, Germany

[3] Laboratory for Electron and Laserscan Microscopy, Leibniz Institute for Neurobiology, 39118 Magdeburg, Germany

[4] Institute of Biochemistry and Cell Biology, Medical Faculty, Otto-von-Guericke-University, 39120 Magdeburg, Germany

[5] German Resilience Center, University Medical Center of the Johannes Gutenberg University, 55128 Mainz, Germany

[6] Center for Behavioral Brain Sciences (CBBS), 39120 Magdeburg, Germany

[7] Department of Informatics and Microsystem Technology, University of Applied Sciences Kaiserslautern, 66482 Zweibruecken, Germany

vesicles are to date unexplored. Using overexpression of GFP-tagged BDNF, it was suggested that BDNF is released either constitutively or in an activity-dependent manner [6–12]. The activity-dependent release of BDNF is assumed to be a key mechanism for the induction and expression of synaptic plasticity in many areas of the mammalian brain [3, 13]. Similar to other neuropeptides and secreted proteins, BDNF synthesis and post-translational modifications involve intracellular trafficking and processing of BDNF in the endoplasmic reticulum (ER), Golgi apparatus, and trans-Golgi network (TGN). Accordingly, BDNF protein is assumed to be stored in TGN-derived secretory vesicles that undergo exocytosis in response to electrical activity-driven rise of intracellular Ca^{2+} levels [10].

In fixed tissue, BDNF protein has been detected by immunohistochemistry in somata, axons, dendrites, and spines of mammalian neurons, e.g., in hippocampus, cortex, and amygdala [14–18]. Likewise, overexpression of GFP-labeled BDNF suggested dendritic as well as axonal targeting of BDNF vesicles [8, 9, 11, 19], and the presence of BDNF vesicles in spines [13, 18]. However, whether this localization reflects the targeting of *endogenous* BDNF in intact neurons under physiological conditions is unknown.

In this study, we set out to address the localization of *endogenous* BDNF-GFP vesicles in living brain slices as well as the exocytosis of BDNF-GFP containing vesicles with a method that does neither rely on potentially unspecific BDNF antibody detection nor on overexpression of fluorescent protein-labeled BDNF. To reach this aim, we generated a knock-in mouse model in which the *endogenous* BDNF exon 9 (coding for the entire protein) is replaced by BDNF-GFP. This mouse expresses BDNF-GFP under the control of the unaltered BDNF gene regulatory elements and allows detection of *endogenous* BDNF by the inherent GFP fluorescence of the fusion protein. Our analysis provides novel insights into the strong dendritic targeting and the unexpectedly slow kinetics of exocytosis of single vesicles containing *endogenous* BDNF.

Our study provides a proof of concept that C-terminal knock-in of GFP into secreted proteins can be used to visualize their release in vivo.

Results

Targeting Construct to Replace *Endogenous* BDNF with BDNF-GFP on Chromosome 2 of the Mouse Genome

The mouse BDNF gene is located on chromosome 2 and contains eight 5′ non-coding exons and one 3′ coding exon (exon 9 [20]). This exon 9 is translated into protein and contains the entire pre-pro-BDNF sequence. BDNF mRNA transcripts consist of either of the 5′ exons 1–8 that are spliced to the protein encoding exon 9. Expression of the different transcripts is regulated in an activity-dependent fashion by specific promoter regions upstream of exons 1–8, respectively. Due to alternative splicing and polyadenylation, at least 18 distinct mRNA species were identified in mice with either short or long 3′UTR [20]. To enable detection of BDNF by endogenous GFP fluorescence, we generated a targeting construct consisting of the mouse BDNF exon 9 sequence fused at its C-terminus in frame to the enhanced GFP (EGFP) coding sequence (compare [21]). This targeting vector contained the left (1.63 kb) and the right (4.84 kb) arm of homology of the mouse BDNF gene. The exon 9 sequence flanked BDNF-GFP with 21 bp to the 5′ and 2.82 kb to the 3′, thus, comprising approximately half of the sequence of the right homology arm (see Fig. 1a). After homologous recombination in ES cells, blastocyst injection, and germline transmission of the construct, we obtained homozygous knock-in BDNF-EGFP (KiBE) mice. In these KiBE mice, the wt BDNF coding sequence on chromosome 2 is replaced by BDNF-GFP, thus driving the expression of green fluorescent BDNF under the control of the *endogenous* BDNF gene regulatory elements. Accordingly, all BDNF expressed in these mice is directly visible by the now endogenous EGFP fluorescence. Male and female heterozygous KiBE mice ($KiBE^{+/-}$) were mated and gave rise to homozygous KiBE animals ($KiBE^{+/+}$). Heterozygous and homozygous KiBE mice develop normally without any obvious defects compared to their wt littermates, including intact BDNF-dependent LTP in the CA1 area of the hippocampus (Suppl. Fig.1). Moreover, we did not observe any deficits in long-term survival of KiBE mice that reach an age of 15 months and beyond (Suppl. Fig.1).

Western Blot Analysis of BDNF-GFP Expression

To check the expression level and posttranslational modifications of BDNF in KiBE mice, whole brain lysates of heterozygous and homozygous animals as well as their wt littermates were subjected to western blot analysis (Fig. 1b–e). Using an anti-BDNF antibody, we detected pro-BDNF with an apparent molecular weight of 32 kD and mature BDNF (mBDNF) as a 14-kD band, being consistent with published values for wt BDNF (see e.g., [22]). As expected, both bands were absent from lysates of homozygous KiBE animals and from homozygous BDNF knockouts (used as negative controls; compare Fig. 1b). In lysates from KiBE animals, the BDNF antibody detected an additional band at 58 kD reflecting the pro-BDNF-GFP variant inserted by the knock-in procedure (compare [6, 19]). At the expected position for mature BDNF-GFP (mBDNF-GFP; mBE) at 43 kD and also at 26 kD, the BDNF antibody detected unspecific non-BDNF-related bands that were also present in lysates of homozygous BDNF ko mice. The unspecific band at 43 kD was previously reported in mammalian cells (compare e.g., [19]) and prevented the proper detection of mBDNF-GFP at the same

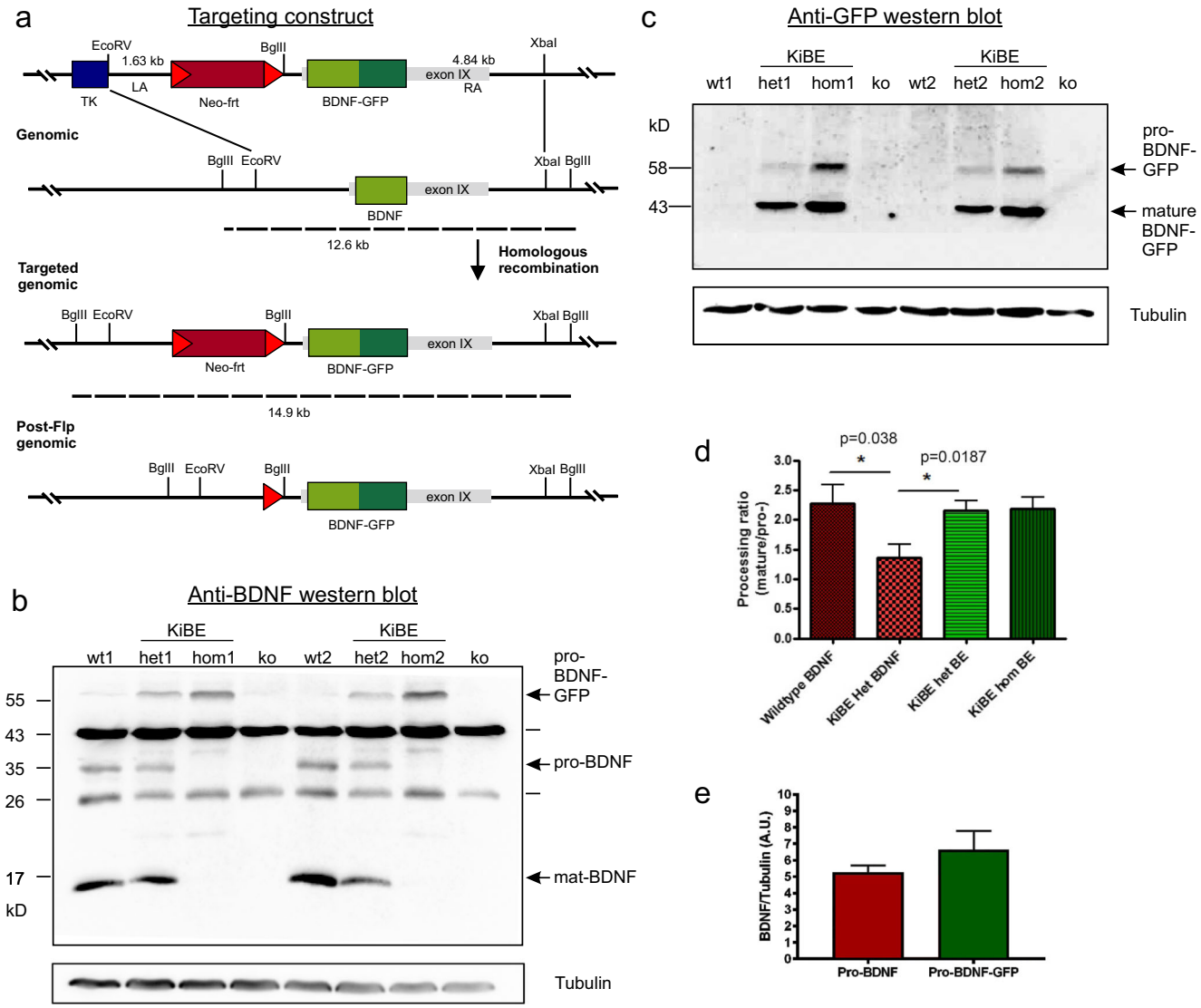

Fig. 1 Targeting construct and BDNF western blots. **a** BDNF-GFP knock-in mouse targeting strategy. Targeting construct harboring the left arm (LA) and right arm (RA) to mediate homologous recombination, the BDNF-GFP sequence, and 5′ a frt-flanked neomycin resistance (Neo-frt) as well as a HSV-TK cassette (TK). Homologous recombination took place between EcoRV and XbaI site of the genomic locus, whereas BglII sites were used for Southern Blot analysis of the targeted genomic locus. After crossbreeding with flipase (Flp) deleter mice, the post-Flp genomic locus still harbors one frt site 5′ to the introduced BglII site. Exon IX is delineated as a light gray box flanking BDNF-GFP sequence. **b** Anti-BDNF western blot analysis of wt BDNF and BDNF-GFP (BE) in hippocampus lysates from heterozygous (het1, het2) and homozygous KiBE mice (hom1, hom2), compared to wt littermates and homozygous BDNF ko mice (ko, negative control). The arrows indicate the expected positions for pro-BDNF-GFP, pro-BDNF, and mature BDNF. **c** Anti-GFP western blot analysis of BDNF-GFP in hippocampus lysates of heterozygous and homozygous KiBE mice, compared to wt littermates and homozygous BDNF ko mice. **d** Quantitative analysis of western blots as shown in (**b**) and (**c**): ratio of mature BDNF vs. pro-BDNF in hippocampal lysates of wt and heterozygous KiBE mice (red bars), and ratio of mature BDNF-GFP vs. pro-BDNF-GFP in heterozygous and homozygous KiBE mice ($n = 8$ animals). **e** Densitometric quantification of pro-BDNF and pro-BDNF-GFP after detection with the anti-BDNF antibody compared to the respective tubulin signal, $n = 4$ wild-type and 4 homozygous KiBE mice

position. However, probing the blots with an anti-GFP antibody allowed to clearly detect pro-BDNF-GFP at 58 kD and mBDNF-GFP at 43 kD, being consistent with the results from the BDNF western blots (Fig. 1c–e).

Since pro-BDNF and mBDNF both exert distinctly different and partially even opposing biological functions (for a recent review see [23]), the pro-BDNF/mBDNF ratio critically determines intact development and proper adult nervous system function. Using the BDNF antibody, we determined a mature/pro-BDNF ratio of 2.25 ± 0.32 ($n = 8$) in wt mice (Fig. 1d). Likewise, using the GFP antibody, we detected a mature/pro-BDNF-GFP ratio of 2.19 ± 0.19 in homozygous KiBE mice ($KiBE^{+/+}$, $n = 8$), which was not significantly different from the respective ratio in wt mice. These results suggest that the C-terminal GFP tag does not affect the proper processing of pro-BDNF-GFP by protein convertases and

other intra- and extracellular proteinases known to contribute to cleavage of pro-neurotrophins to their mature counterparts (reviewed e.g. in [24]). However, in heterozygous KiBE mice, we detected less efficient conversion of pro-BDNF to mature BDNF, whereas the pro-BDNF-GFP to mature BDNF-GFP ratio remained unaffected in the same animals (Fig. 1d). This might indicate competition between both BDNF species for protein convertase binding sites.

When comparing pro-BDNF bands in wt mice with pro-BDNF-GFP bands in homozygous KiBE animals in the same blots, we observed similar intensities (Fig. 1b) and obtained no significant difference in expression level when compared to tubulin (Fig. 1e). Together with the unchanged ratio of mature/pro-BDNF-GFP (Fig. 1d), these results suggest that the expression level of BDNF-GFP in homozygous KiBE$^{+/+}$ mice is comparable with the expression of untagged BDNF in wt mice.

Expression Pattern of BDNF-GFP in the Hippocampus of BDNF-GFP Knock-in Mice

Using confocal and bright field microscopy, BDNF-GFP was detected in hippocampal brain slices of KiBE mice subjected to anti-GFP immunohistochemistry (Fig. 2a, b; Suppl. Fig.2). BDNF-GFP immunoreactivity was visible most prominently in the pyramidal cell layer of CA3, in the granule cell layer of the dentate gyrus (DG), and in neurons of the hilar region (CA4). Moreover, BDNF-GFP immunoreactivity was clearly detected in the pyramidal cells in CA1 (Suppl. Fig.2a), albeit in a lower percentage of cells as compared to CA3, and with slightly lower intensity per cell compared to the CA3 area. BDNF-GFP expression was restricted to the soma (excluding the nucleus) and extended in CA3 neurons most obviously into proximal dendrites (approx. 30 μm; Suppl. Fig.2c). Using amplification of the GFP antibody signal by enzymatic labelling with an avidin-biotin-peroxidase-complex followed by diaminobenzidine (DAB) conversion yielded similar results (Suppl. Fig.2e). This somato-dendritic pattern of BDNF-GFP localization in hippocampal subfields was observed in all sections (> 20) of the 8 homozygous KiBE mice processed independently for anti-GFP IHC.

Most importantly, also the *endogenous* BDNF-GFP fluorescence was clearly detectable in the hippocampus without the need to use any labeling or amplification procedures (Fig. 2c–f; observed in 15 of 15 slices from 6 homozygous KiBE mice). Although the signal strength (signal/noise ratio) was slightly lower than observed in anti-GFP IHC experiments, the distribution within cells throughout all hippocampal subfields was indistinguishable from the IHC results (compare Fig. 2 and Suppl. Fig.2). Taken together, this BDNF-GFP distribution in KiBE mice is in line with previous results obtained with BDNF antibody staining in rats and mice (see e.g., [14, 17]), suggesting that the expression pattern of BDNF-GFP in different hippocampal subfields and regarding the somato-dendritic targeting is apparently not altered by the GFP tag.

Cellular Localization of BDNF-GFP in Brain Slices of BDNF-GFP Knock-in Mice

Using confocal imaging in brain slices of young adult (2–3 months old) KiBE mice, we next determined axonal vs. somato-dendritic targeting of BDNF-GFP by counterstaining with antibodies directed against dendritic (MAP2) and axonal marker proteins (SMI 312). We observed colocalization of the *endogenous* BDNF-GFP fluorescence with MAP2 in the perinuclear somatic region (arrowheads) and in proximal dendrites (arrows) in all hippocampal subfields (see Fig. 3a). The BDNF-GFP fluorescence did not colocalize with the axonal marker SMI312 (Fig. 3b), being consistent with localization of BDNF-GFP in the soma and proximal dendrites of CA1 and CA3 pyramidal neurons rather than in adjacent axons innervating the soma area.

Most importantly, localization of *endogenous* BDNF-GFP could also be determined in vital acute transversal hippocampal slices ex vivo using confocal imaging of λ-stacks followed by linear unmixing (Fig. 4). This unmixing procedure was used to better distinguish GFP signals from green background fluorescence. The pattern of GFP fluorescence observed in living slices (KiBE$^{+/+}$ CA1: 12 slices/9 animals, CA3: 11 slices/8 animals, DG: 12 slices/9 animals; WT littermates CA1: 9 slices/7 animals, CA3: 11 slices/7 animals, DG: 11 slices/8 animals) resembled in all subfields of the hippocampus very much the results obtained in fixed slices (Figs. 2 and 3; Suppl. Fig.2), with BDNF-GFP most prominently expressed in the somato-dendritic compartment of the pyramidal cell layer in CA3 (Fig. 4b), in the granule cell layer, the hilar region of the dentate gyrus (Fig. 4c), and in the pyramidal cell layer of CA1 (Fig. 4a). These recordings in acute hippocampal slices revealed dendritic BDNF-GFP vesicles also in distal apical dendrites of CA3 and CA1 pyramidal neurons (Fig. 4, arrows), proving for the first time the existence of *endogenous* BDNF-containing vesicles in pyramidal cell dendrites in living hippocampal slices.

Subcellular Localization of BDNF-GFP Vesicles Using Super Resolution Microscopy in Cultured Hippocampal Neurons of BDNF-GFP Knock-in Mice

To allow exact subcellular allocation of BDNF-GFP vesicles to different cellular compartments, we performed colocalization studies with different axonal, dendritic, and synaptic markers in cultured hippocampal neurons from homozygous KiBE mice (Suppl. Fig.3). Staining of homozygous KiBE neurons with the same anti-GFP antibody used for hippocampal slices (compare Fig. 2, Suppl. Fig.2) showed complete colocalization of BDNF-

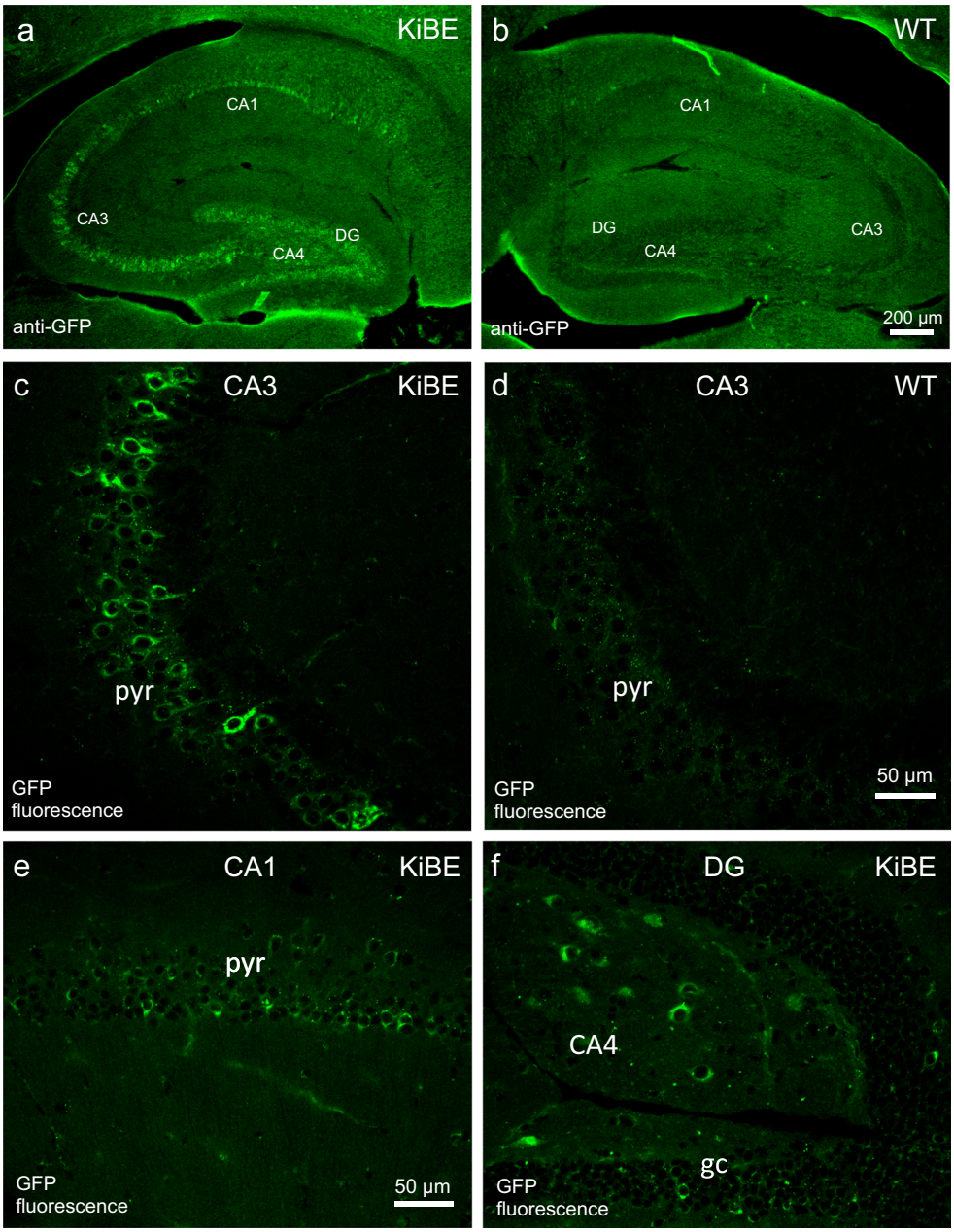

Fig. 2 Detection of BDNF-GFP in different hippocampal subfields. **a**, **b** Anti-GFP immunofluorescent detection of BDNF-GFP in homozygous KiBE mouse hippocampal slices (left) vs. wt littermate control (right) at low magnification. GFP immunopositive cells are most numerous in the CA3 layer and in the DG area but are also clearly visible in CA1. **c**–**f** Confocal imaging followed by linear unmixing of *endogenous* BDNF-GFP fluorescence in different hippocampal subfields as denoted. **c**, **d** CA3 area of homozygous KiBE mice compared to wt littermate control. *Endogenous* BDNF-GFP fluorescence in CA3 pyramidal neurons (pyr) shows somato-dendritic localization of BDNF-GFP whereas no such GFP fluorescence is visible in wt controls. **e**, **f** BDNF-GFP fluorescence was also detected in CA1 pyramidal neurons (**e**) as well as in hilar mossy cells (in CA4 area) and granule cells (gc) in the DG (**f**), and showed a similar subcellular localization as in CA3 (compare Suppl. Fig.2)

GFP fluorescence with the GFP antibody, and absence of unspecific staining in axons and dendrites of wt littermates. The punctate structures observed in the neuronal processes of KiBE neurons resembled BDNF vesicles previously described in BDNF-GFP overexpressing hippocampal neurons [6, 19]. Counterstaining of KiBE neurons with MAP2 antibodies revealed that the majority of these BDNF-GFP vesicles were located within dendrites (Suppl. Fig.3a). Co-staining of KiBE neurons with antibodies directed against the presynaptic marker Bassoon disclosed rare but clearly existing colocalization, whereas we observed a more frequent colocalization with the postsynaptic marker of glutamatergic synapses PSD95.

To better resolve dendritic and axonal targeting of BDNF-GFP vesicles, KiBE mouse hippocampal cultures were counterstained with antibodies directed against different markers and imaged with STED microscopy (Figs. 5, 6, 7, and 8). Staining with an antibody detecting the axonal marker SMI 312 (Fig. 5) showed decoration of dendrites of the cultured neurons with SMI 312-positive presynaptic boutons and axonal segments running partially attached to dendrites (see e.g., Fig. 5a, ROI 1). In the same neuron, another dendrite not colocalizing with SMI 312, which is therefore not attached to an axon, can be clearly identified (Fig. 5a, ROI 2). This pattern of axon-attached as well as axon-free dendrites was a typical finding in all cultured KiBE$^{+/+}$ neurons investigated

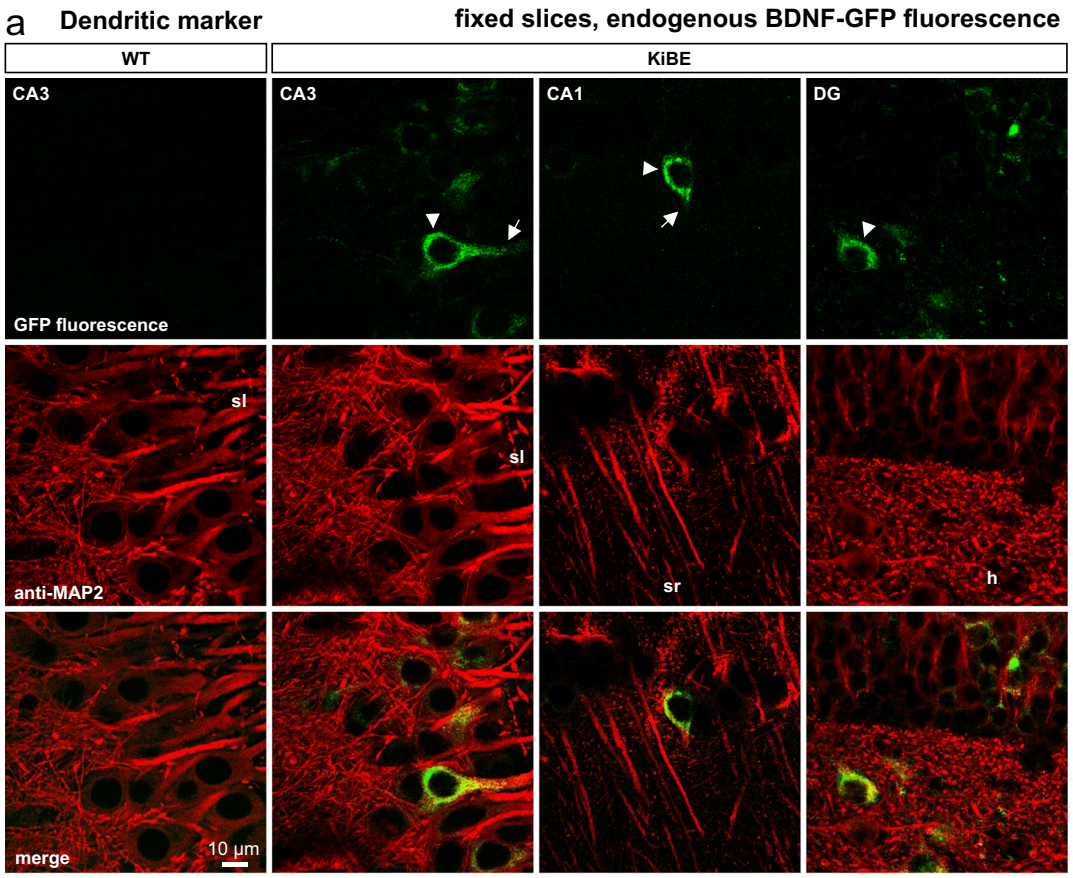
a
Dendritic marker
fixed slices, endogenous BDNF-GFP fluorescence
WT
KiBE
CA3
CA3
CA1
DG
GFP fluorescence
sl
sl
sr
h
anti-MAP2
merge
10 µm

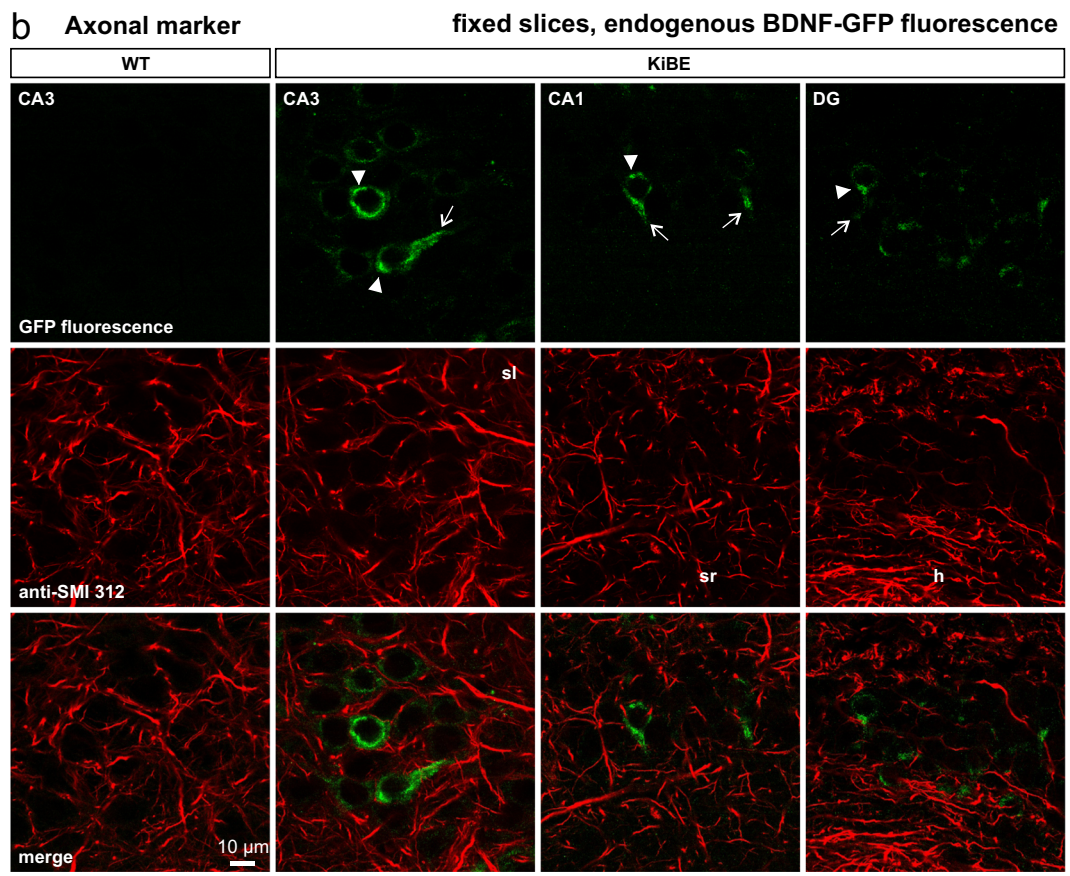
b
Axonal marker
fixed slices, endogenous BDNF-GFP fluorescence
WT
KiBE
CA3
CA3
CA1
DG
GFP fluorescence
sl
sr
h
anti-SMI 312
merge
10 µm

◀ **Fig. 3** *Endogenous* BDNF-GFP fluorescence reveals subcellular localization of BDNF-GFP vesicles in dendrites in different hippocampal subfields. **a** *Right*: BDNF-GFP fluorescence observed with linear unmixing in adult homozygous KiBE mice in CA3 pyramidal cells, CA1 pyramidal cells, and in DG granule cells, compared to wt littermates CA3 neurons (*left*). *Middle panel*: anti-MAP2 immunofluorescent (red) detection of dendrites. *Lower panel*: merged GFP and red anti-MAP2 fluorescence. Note the localization of BDNF-GFP fluorescence in soma (white arrowheads) and dendrites (white arrows) of the different types of excitatory hippocampal neurons. **b** *Right*: BDNF-GFP fluorescence observed with linear unmixing in adult homozygous KiBE mice in CA3 pyramidal cells, CA1 pyramidal cells, and in DG granule cells, compared to wt littermates CA3 neurons (*left*). *Middle panel*: anti-SMI 312 immunofluorescent detection of axons. *Lower panel*: merged GFP and red anti-SMI 312 signal. Note the absence of axonal BDNF-GFP signals in the different BDNF-GFP expressing excitatory hippocampal neurons, whereas somata (white arrowheads) and dendrites (white arrows) contain BDNF-GFP vesicles (sr: stratum radiatum, sl: stratum lucidum, h: hilus)

and has been reported previously by others [25]. When looking with STED imaging at axon-free dendritic stretches at higher magnification (Fig. 5c), we can unequivocally assign the BDNF-GFP vesicles in ROI 2 of this neuron to being dendritic. In case of ROI 1, we most likely observed an axon attached to the BDNF-GFP vesicle-containing dendrite. However, given the very close association of vesicles with SMI 312 puncta in the STED images, we cannot exclude that some of the vesicles in ROI 1 are also present in the attached axon.

Figure 6 shows the corresponding results of the STED analysis for co-staining with antibodies detecting the dendritic marker MAP2. BDNF-GFP vesicles were present in all 3 proximal dendrites. STED analysis of ROI 1 in such a dendrite revealed the presence of BDNF-GFP vesicles throughout the whole width and length of the dendrite (Fig. 6a–c). Also, some of these BDNF-GFP vesicles completely colocalized with the MAP2 spots even at this super resolution (Fig. 6c, left). This intimate colocalization of BDNF-GFP and MAP2 signals can only be reconciled with many of the vesicles being present inside of the dendrite rather than in a hypothetical attached axon. Importantly, we could also recognize a stretch of the axon of this neuron, identified by the absence of MAP2 co-staining (Fig. 6a, ROI 2). Obviously, there are some vesicles present also in this process, suggesting that also in this neuron, some additional BDNF-GFP vesicles can be found in the presumed axon. To quantify the dendritic localization of BDNF-GFP vesicles, anti-MAP2 STED image z-stacks of all neuronal processes of cells as shown in Fig. 6 were analyzed (see Experimental Procedures). This quantification (11 z-stacks from 4 KiBE mouse neurons were analyzed) revealed that 70.6 ± 4.1% of the vesicles were contained within MAP2 delimited dendritic structures, matching the percentage of dendritic BDNF-GFP vesicles in hippocampal neurons overexpressing BDNF-GFP [6]. Thus, dendritic localization of BDNF-GFP vesicles expressed under the control of the *endogenous* BDNF gene regulatory elements seems to prevail in KiBE mouse derived dissociated hippocampal cultures. Of note, this dendritic localization of BDNF-GFP vesicles is also observed in acute and fixed KiBE mouse hippocampal slices (compare Figs. 2, 3, and 4).

To assess the synaptic localization of BDNF-GFP, we counterstained KiBE mouse hippocampal cultures with antibodies directed against pre- and postsynaptic markers. Anti-PSD95 immunocytochemistry performed under the same STED z-stack recording conditions as described above allowed us to detect very closely apposed signals for PSD95 spots and BDNF-GFP vesicles at numerous locations within the dendrites (Fig. 7), being consistent with prevalent dendritic targeting of BDNF-GFP vesicles in our hippocampal neurons (compare Fig. 6). In a final STED analysis, we aimed at determining colocalization of BDNF-GFP vesicles with the presynaptic marker Bassoon. Here, Bassoon-positive puncta decorated BDNF-GFP vesicle-containing dendrites of KiBE neurons (Fig. 8a). When imaging with STED resolution, many Bassoon puncta were found in the neighborhood of BDNF-GFP vesicles. To determine the proximity of PSD95 and Bassoon, respectively, to BDNF-GFP vesicles, we quantified the colocalization in the images (see Experimental Procedures). Nearest neighbor analysis of BDNF-GFP vesicles in relation to PSD95-positive vs. Bassoon-positive puncta (Suppl. Fig.4) revealed no significant difference between BDNF-GFP vesicle proximity to the presynaptic or the postsynaptic marker. The long tails in the nearest neighbor analysis for both markers suggest that BDNF-GFP vesicles are not specifically clustered at either presynaptic release sites or close to the postsynaptic membrane (Suppl. Fig.4c).

Altogether, our colocalization experiments (i.e., Figs. 5, 6, 7, and 8) suggest a strong dendritic localization of BDNF-GFP vesicles in the vicinity of postsynaptic structures in hippocampal neurons. In many neurons, we also find indications for additional axonal localization of BDNF vesicles, which is, however, less prominent than dendritic targeting.

The high magnification STED images obtained for experiments as shown in Figs. 5, 6, 7, and 8 were also used to approximate the size of BDNF-GFP granules, and yielded an apparent vesicle diameter of 50–100 nm. This suggests that BDNF-GFP vesicles are only slightly larger than small clear transmitter vesicles.

Live Cell Imaging of BDNF-GFP Vesicles in Hippocampal Neurons of BDNF-GFP Knock-in Mice

Low density hippocampal microcultures of homozygous KiBE animals were recorded at 14 DIV using epifluorescence microscopy, as described previously [26]. In a first series of experiments, we compared distribution and characteristics of BDNF-GFP vesicles in homozygous and heterozygous KiBE mice with results obtained when overexpressing BDNF-GFP

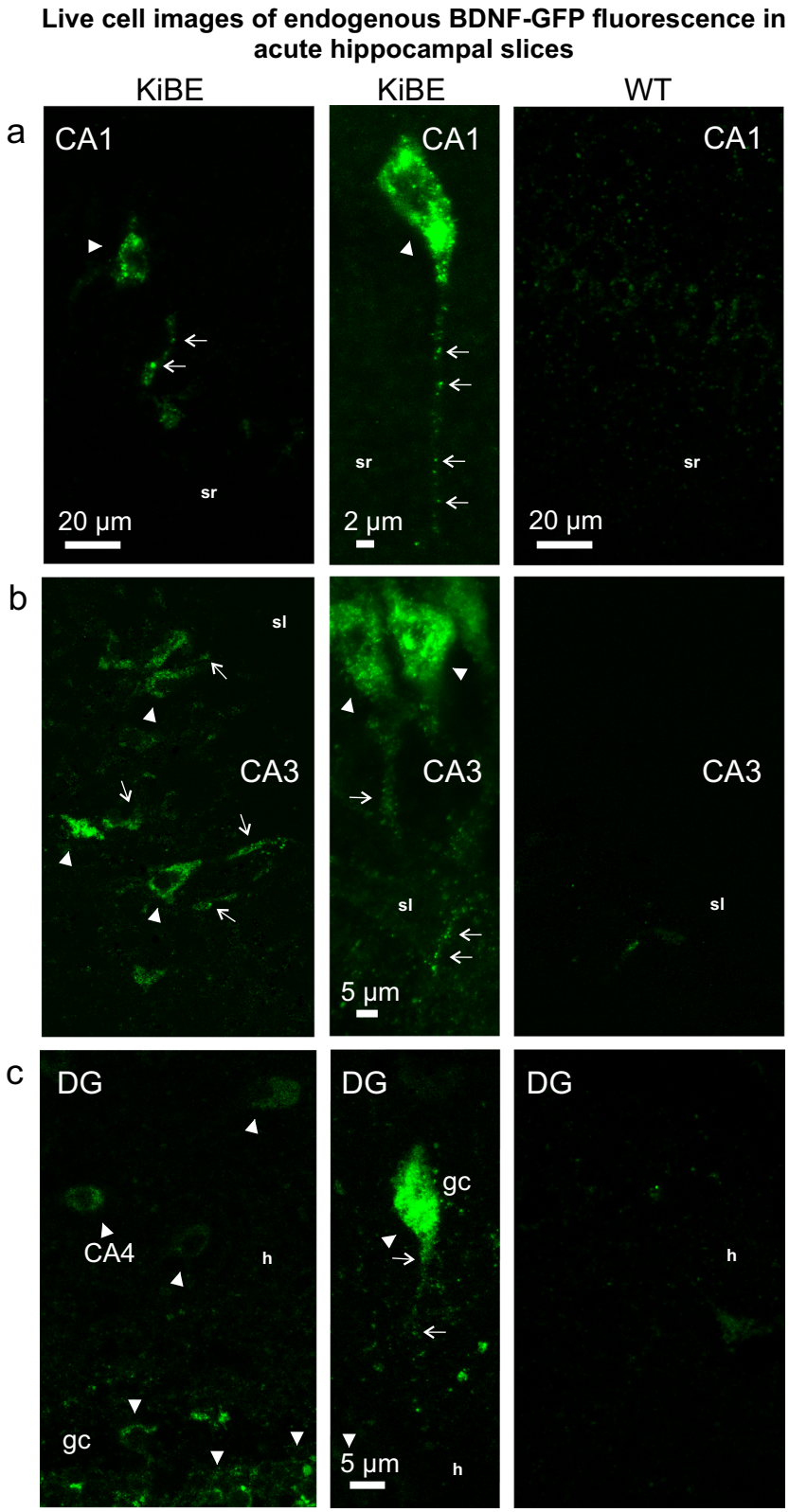

Fig. 4 Live cell imaging of BDNF-GFP vesicles in dendrites of acutely isolated native hippocampal slices from homozygous KiBE mice. **a–c** Confocal images of *endogenous* BDNF-GFP fluorescence in homozygous KiBE mice (*left*), age-matched wt littermates (*right*), and higher magnification views (middle; different slices than on the left) of BDNF-GFP expressing CA1 and CA3 pyramidal neurons, and dentate gyrus granule cells. Transversal hippocampal slices were isolated from 2 to 3 months old homozygous KiBE mice or wt littermate controls, and continuously superfused with 5%CO_2/95% O_2 equilibrated artificial cerebrospinal fluid (ACSF). The depicted regions (CA1 pyramidal cell layer, CA3 pyramidal cell layer, dentate gyrus granule cell layer) in these acute hippocampal slices show patterns of BDNF-GFP vesicle distribution that are reminiscent of results obtained with anti-GFP immunohistochemistry in fixed slices (sr: stratum radiatum, sl: stratum lucidum, h: hilus). Confocal images were analyzed using linear unmixing as described in the Experimental Procedures section. Note the BDNF-GFP vesicles in the soma (white arrowheads) and in dendrites (white arrows) in CA1, CA3, and DG neurons (lower part: granule cells; upper part: hilar mossy cells in CA4)

in wt hippocampal neurons (Suppl. Fig.5). Incubation of KiBE mouse neurons with 5 mM NH_4Cl, which neutralizes intravesicular pH thereby unquenching GFP, elicited a roughly 2.4-fold increase in BDNF-GFP fluorescence (Suppl. Fig.5d). This is almost identical to the 2.2-fold respective increase observed for BDNF-GFP overexpressing wt neurons [26], and implies an intravesicular pH of 5.8 also for *endogenous* BDNF-GFP vesicles in KiBE mice (compare

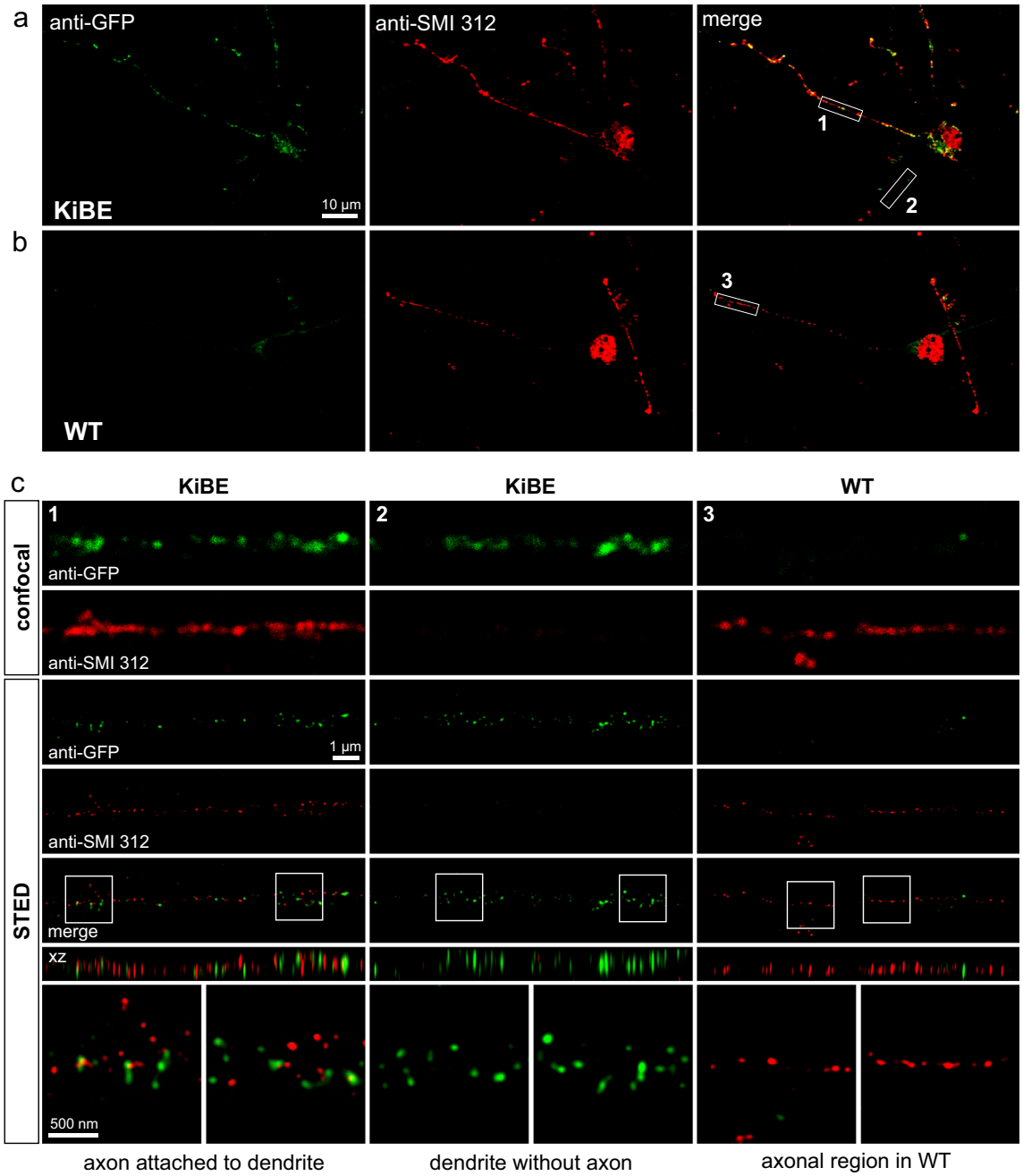

Fig. 5 STED co-imaging of the axonal marker SMI 312 does not reveal prominent localization of BDNF-GFP vesicles in axons of cultured hippocampal KiBE mouse neurons. **a** Confocal image of a homozygous KiBE mouse neuron double immunostained at 7 DIV for GFP and SMI 312, and **b** respective wt control. **c** Confocal and STED images of white boxed regions of interest (ROIs 1–3) marked in (**a**) and (**b**), shown at higher magnification with super resolution microscopy (*merge*: top view (xy); *xz*: side view; lower panel: white boxed regions in merged pictures shown at higher magnification). While at confocal resolution BDNF-GFP vesicles in (**a**) appear to be very close to the axonal SMI 312 staining, STED imaging reveals no prominent colocalization between BDNF-GFP and SMI 312 signals. The yellow signals in (**a**) rather indicate dendritic stretches where SMI 312 positive axons are wrapped around BDNF-GFP vesicle-containing dendrites. STED images of wt neurons (ROI 3) do not show any colocalization of SMI 312 and anti-GFP staining

[26]). Under identical illumination and exposure conditions, average fluorescence intensity of vesicles in neurons from homozygous KiBE mice was twice as high as in heterozygous KiBE animals. This suggests that the loading efficacy of the BDNF-GFP vesicles budding off from the TGN is proportional to the expression level of GFP-tagged BDNF (i.e., ~ 50% fluorescence in vesicles of mice with 1 knock-in allele (heterozygotes) compared to 100% with 2 alleles in homozygotes; Suppl. Fig.5f, g). Interestingly, under identical recording conditions, we found that fluorescence intensity of

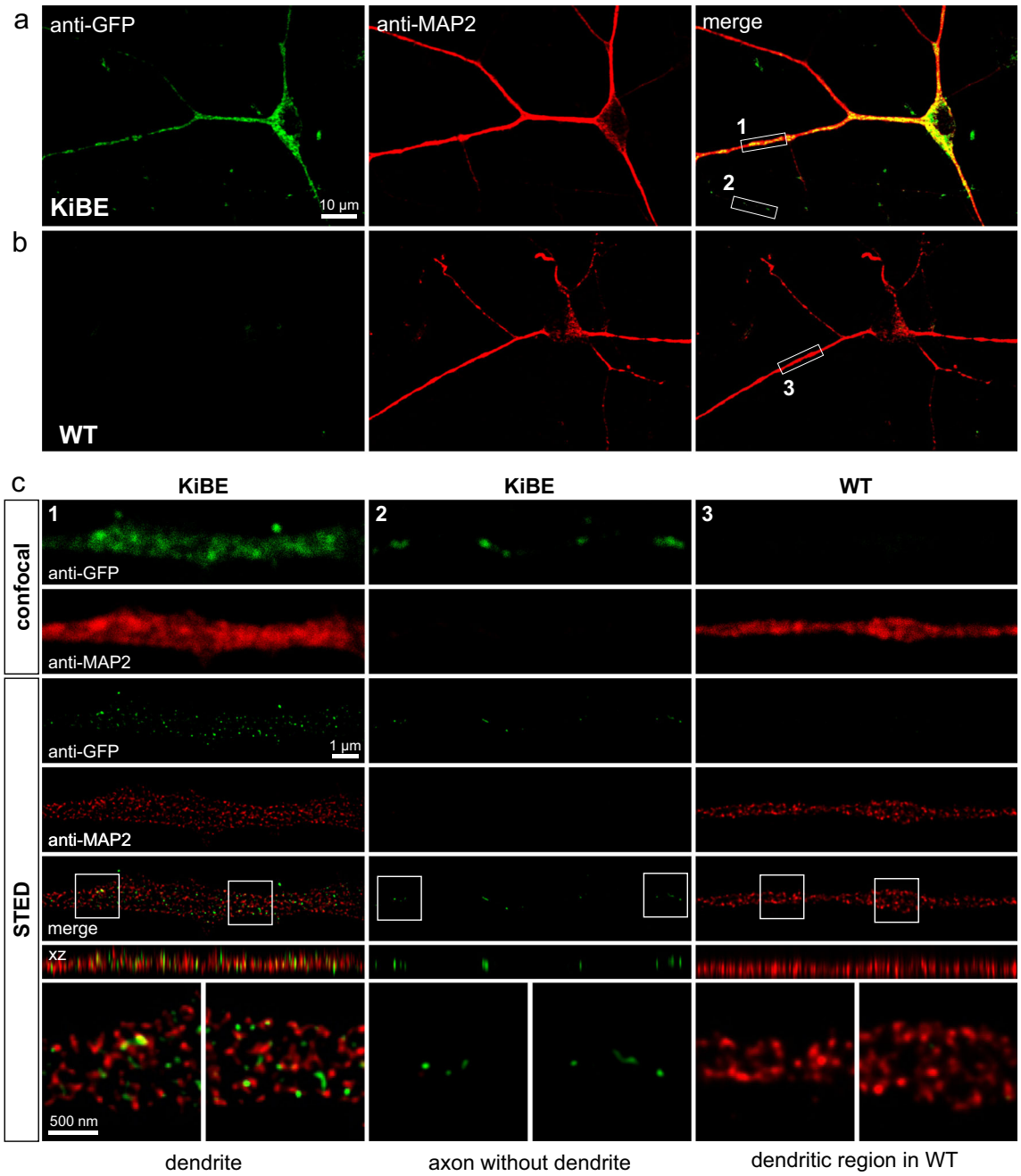

Fig. 6 STED co-imaging of the dendritic marker MAP2 supports the presence of BDNF-GFP vesicles in dendrites of cultured hippocampal KiBE mouse neurons. **a** Confocal image of a homozygous KiBE mouse neuron double immunostained at 7 DIV for GFP and MAP2 and **b** respective wt littermate control. **c** Confocal and STED images of white boxed regions of interest (ROIs 1–3) marked in (**a**) and (**b**), shown at higher magnification with super resolution microscopy (*merge*: top view (xy); *xz*: side view; lower panel: white boxed regions in merged pictures shown at higher magnification). In the KiBE mouse neuron, colocalization of BDNF-GFP and MAP2 is evident in dendrites (ROI 1) but not in axons (ROI 2; identified by absence of MAP2 staining). In wt littermate neurons (ROI 3), there is no colocalization of the red MAP2 staining and any background GFP antibody labeling

vesicles in BDNF-GFP overexpressing wt neurons is roughly 30 times higher than in homozygous KiBE animals (Suppl. Fig.6). Surprisingly, these data indicate that only the concentration of BDNF-GFP in TGN-derived secretory granules strongly depends on BDNF-GFP expression, while neither the size nor the density of BDNF-GFP containing vesicles in neuronal processes are affected (Suppl. Fig.5h, i). It is therefore a challenging task to image BDNF-GFP vesicles in KiBE neurons with good signal to noise ratio.

Next, we analyzed fusion pore opening (FPO) in response to depolarization induced by elevated extracellular potassium (50 mM K^+, see Methods). These measurements were

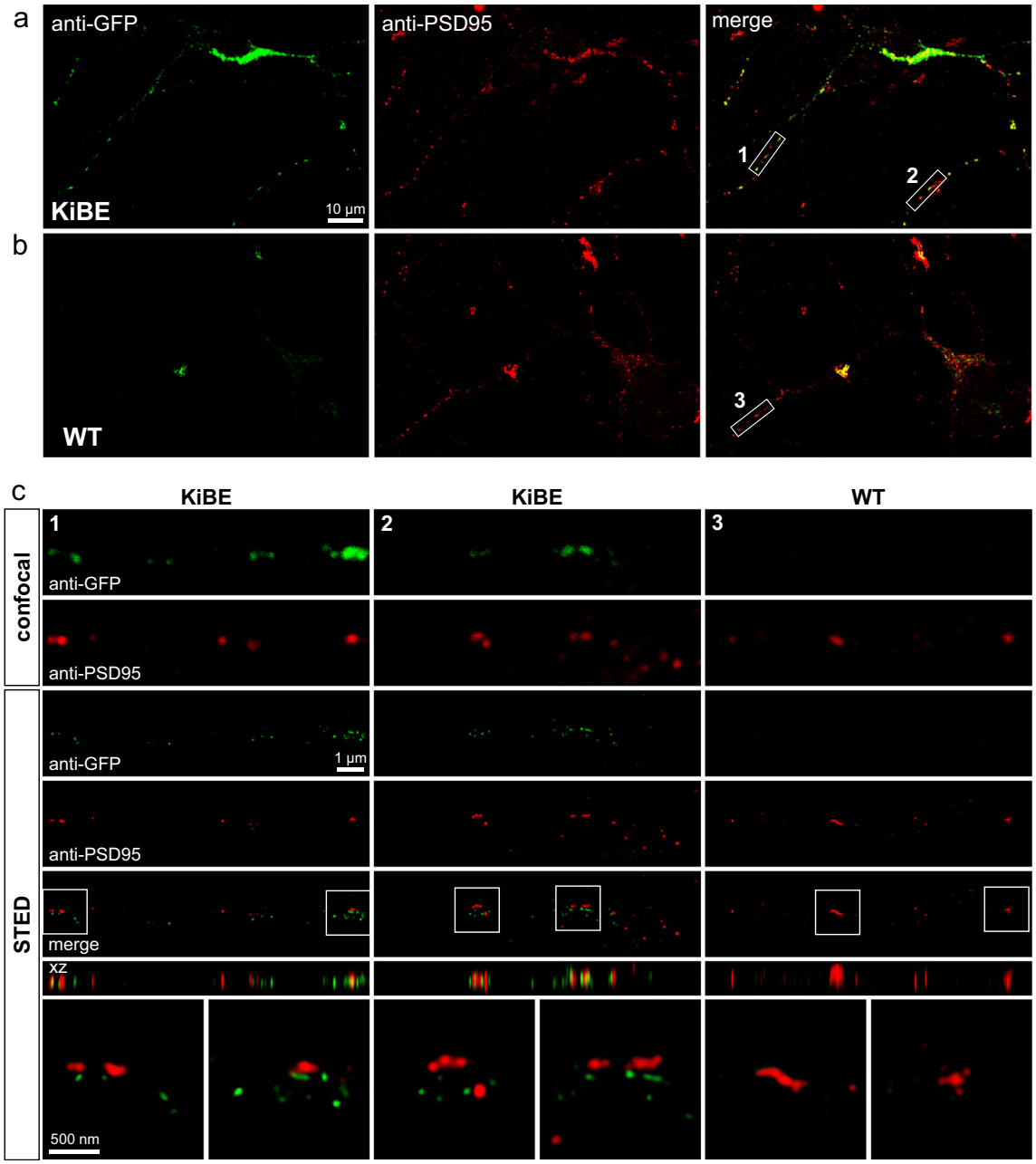

Fig. 7 STED co-imaging of PSD95 reveals BDNF-GFP vesicles in postsynaptic glutamatergic structures of cultured hippocampal KiBE mouse neurons. **a** Confocal image of a homozygous KiBE mouse neuron double immunostained at 7 DIV for GFP and PSD95 and **b** respective wt littermate control. **c** Confocal and STED images of white boxed regions of interest (ROIs 1–3) marked in (**a**) and (**b**), shown at higher magnification with super resolution microscopy (*merge*: top view (xy); *xz*: side view; lower panel: white boxed regions in merged pictures shown at higher magnification). In the KiBE mouse neuron, colocalization of BDNF-GFP and PSD95 is evident in dendrites (ROIs 1 and 2). In the wt littermate neuron (ROI 3), there is no colocalization of the red PSD95 signal and any background GFP antibody labeling

performed in the presence of extracellular bromphenol blue (BPB, 0.3 mM [21]). Under these conditions, single vesicle exocytotic events can be detected as a sudden decrease of vesicular fluorescence intensity after fusion pore opening (FPO), resulting from BPB-induced quenching of intravesicular BDNF-GFP fluorescence (Fig. 9). This sudden decline in fluorescence of individual BDNF-GFP vesicles commenced within 10 s after start of the depolarization, reaching maximum probability at 20–30 s (see Fig. 9f). At the level of vesicle clusters (yellow arrow in Fig. 9b), FPO events in KiBE mouse neurons were visible as a decrease in fluorescence intensity occurring with a similar time course as the single vesicle events (compare Fig. 9c, d). Since such vesicle clusters contain also non-fusing vesicles, the average decline in fluorescence intensity of these clusters (Fig. 9d) is less pronounced than fluorescence decrease of individual

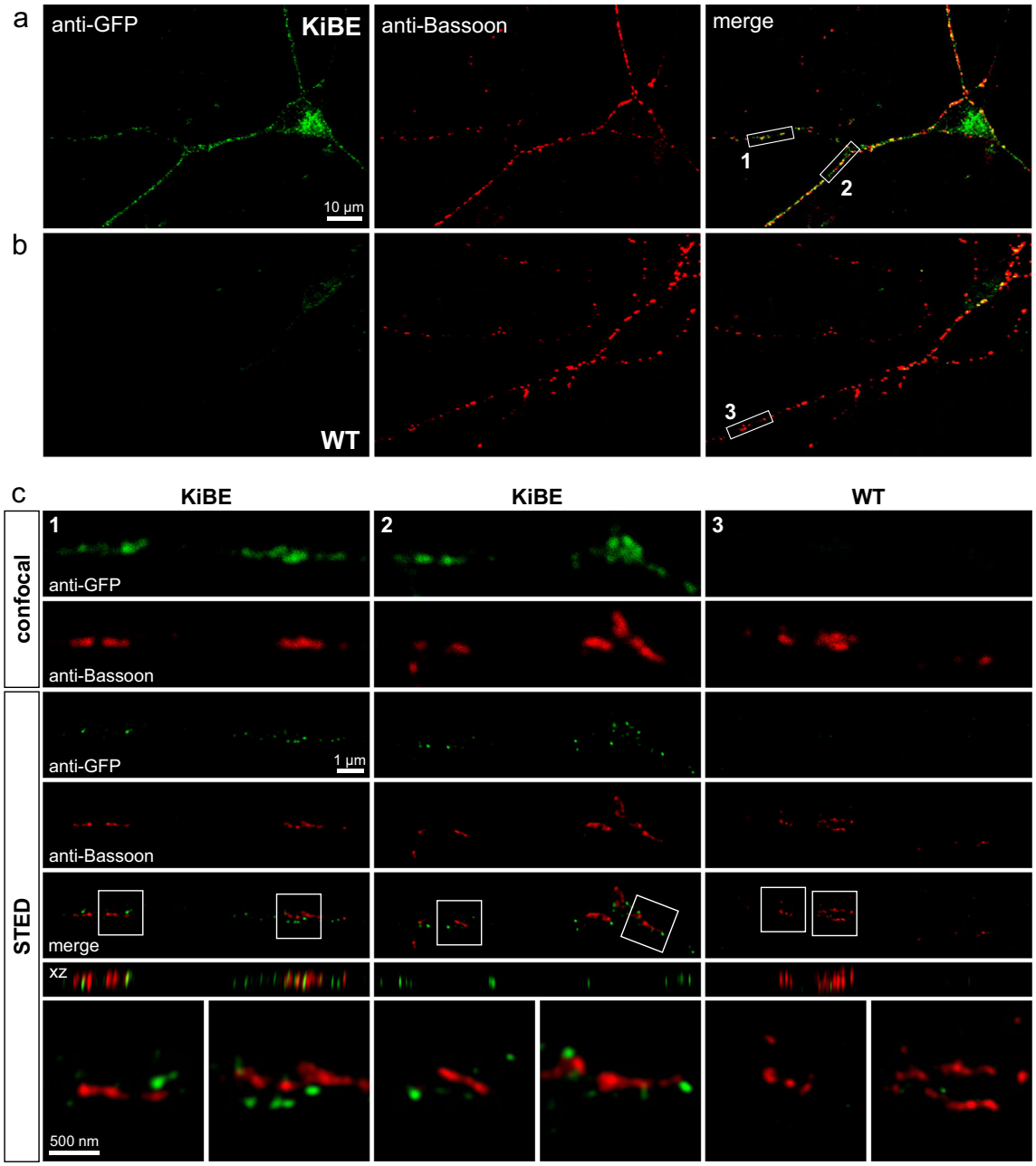

Fig. 8 STED based co-imaging of Bassoon reveals that most BDNF-GFP vesicles are not present in presynaptic terminals of cultured hippocampal KiBE mouse neurons. **a** Confocal image of a homozygous KiBE mouse neuron double immunostained at 7 DIV for GFP and Bassoon and **b** respective wt littermate control. **c** Confocal and STED images of white boxed regions of interest (ROIs 1–3) marked in (**a**) and (**b**), shown at higher magnification with super resolution microscopy (*merge*: top view (xy); *xz*: side view; lower panel: white boxed regions in merged pictures shown at higher magnification). In the KiBE mouse neuron, no exact colocalization of BDNF-GFP and Bassoon is evident (ROIs 1 and 2). The close proximity of some green BDNF-GFP vesicles and the red fluorescence of the presynaptic marker results most likely from the apposition of Bassoon-positive presynaptic terminals with postsynaptic dendritic structures containing BDNF-GFP vesicles. In the wt littermate neuron (ROI 3), there is no colocalization of the red Bassoon signal with any background GFP antibody labeling

fusing vesicles (Fig. 9c). The proportion of dendritic BDNF-GFP vesicles showing depolarization-induced FPO was identical in cultures from heterozygous KiBE$^{+/-}$ and homozygous KiBE$^{+/+}$ mice (Fig. 9f–h). Notably, this percentage was also indistinguishable from the respective results obtained in BDNF-GFP overexpressing hippocampal neurons from wt mice (Fig. 9h). Likewise, the average decline of fluorescence intensity of dendritic vesicle clusters was indistinguishable between the three preparations (Fig. 9e). Overall, this suggests that BDNF-GFP vesicles in KiBE mice are fusion competent

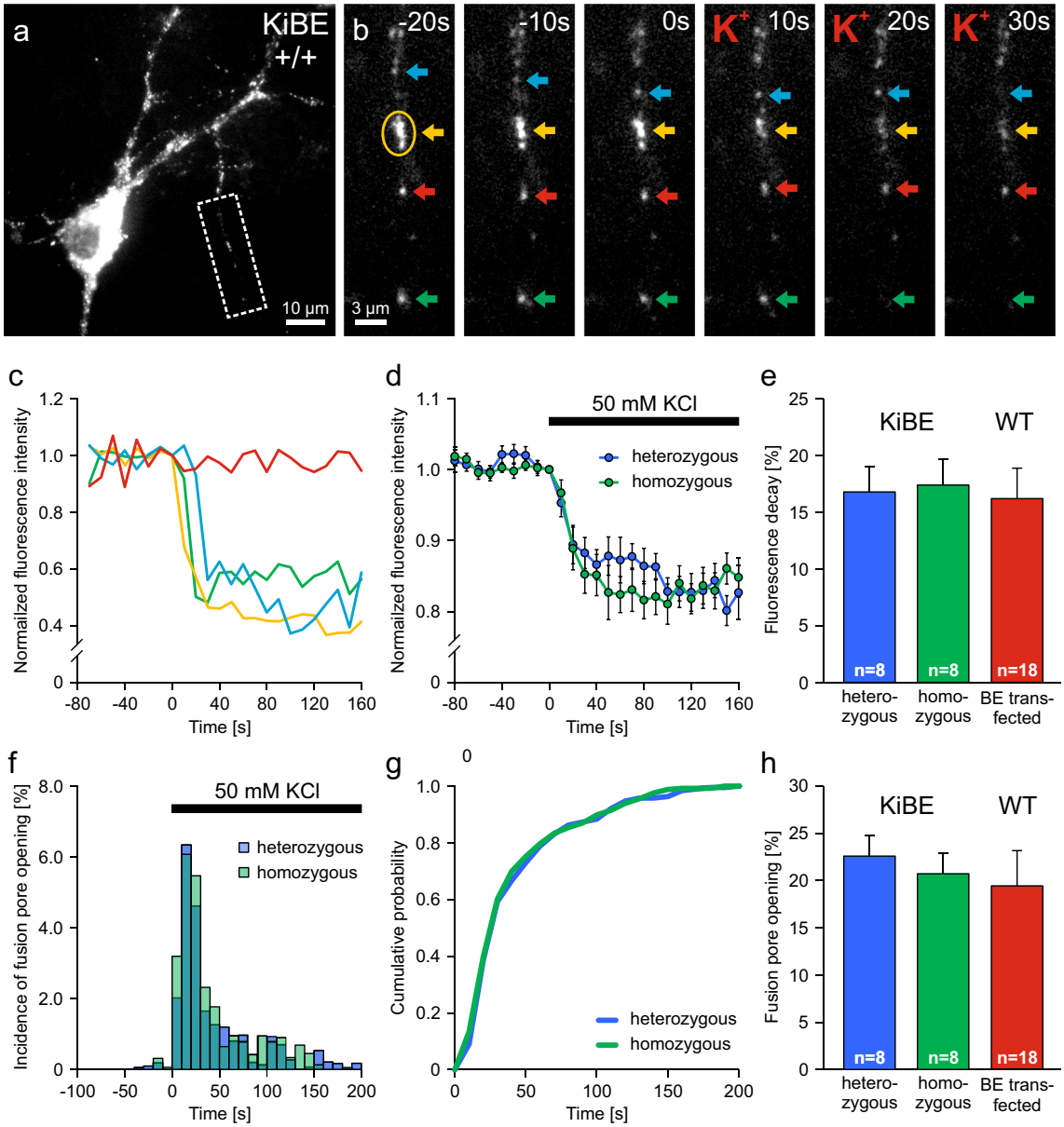

Fig. 9 Measurement of fusion pore openings of BDNF-GFP vesicles in dendrites of cultured hippocampal KiBE mouse neurons. **a** Live cell imaging of elevated K^+ (50 mM) depolarization-induced BDNF-GFP vesicle fusion pore openings (FPOs) in cultured hippocampal neurons from KiBE mice recorded at 14 DIV with epifluorescence microscopy in the presence of the green fluorescence quencher BPB (0.3 mM). **b** White boxed ROI in (**a**) is shown at higher magnification at indicated time points during time lapse movie. Arrows depict individual BDNF-GFP vesicles or vesicle clusters (yellow). **c** Plot of normalized fluorescence intensities of vesicles/clusters marked by colored arrows in (**b**). **d** Average decline in fluorescence intensity of dendritic branches as shown in (**b**) for ROIs in homozygous ($n = 48$) or heterozygous KiBE mouse cultures ($n = 51$). **e** Average amplitude of fluorescence decay after FPO of dendritic branches at 100–160 s after the start of depolarization in (**d**) (heterozygous $KiBE^{+/-}$: 16.8 ± 2.1%; homozygous $KiBE^{+/+}$: 17.4 ± 2.3%; BDNF-GFP (BE) transfected wt neurons: 16.2 ± 2.7%, one-way ANOVA $F_{2,31} = 0.05$, $p = 0.95$). **f** Total FPO events normalized to the total number of vesicles within each region ($KiBE^{+/-}$: 192/856 vesicles showed FPO; $KiBE^{+/+}$: 271/1314 vesicles showed FPO). **g** Cumulative probability plot for data collected as described in (**f**). **h** Total incidence of FPO for KiBE mouse and wt littermate neurons ($KiBE^{+/-}$: 22.6 ± 2.2%; $KiBE^{+/+}$: 20.7 ± 2.2%; BDNF-GFP transfected wt neurons: 19.4 ± 3.7%, one-way ANOVA: $F_{2,31} = 0.18$, $p = 0.83$)

and show similar probability, time course, and quenching responses of fusion pore openings as BDNF-GFP overexpressing neurons from wt mice.

FPO alone is not a direct proof for secretion of vesicle content (i.e., diffusion of the vesicle cargo into the extracellular space). Therefore, we next investigated BDNF-GFP release that can be monitored as the decrease in fluorescence intensity of BDNF-GFP containing vesicles after FPO in the absence of BPB. Since intravesicular pH of secretory granules in hippocampal neurons amounts to 5.8 [26], FPO

under these conditions is visible as a sudden increase in fluorescence intensity, due to unquenching of GFP fluorescence when intravesicular pH equilibrates to the extracellular pH of 7.4 (Supplemental movie 1). Indeed, depolarization of KiBE mouse hippocampal neurons led to a FPO induced sudden increase in fluorescence intensity that was followed by a mono-exponential decay reflecting release of BDNF-GFP (Fig. 10a–c). Note the large scatter in the delay of FPO followed by subsequent cargo release between individual vesicles in the same dendrite (Fig. 10c). Neither the FPO associated

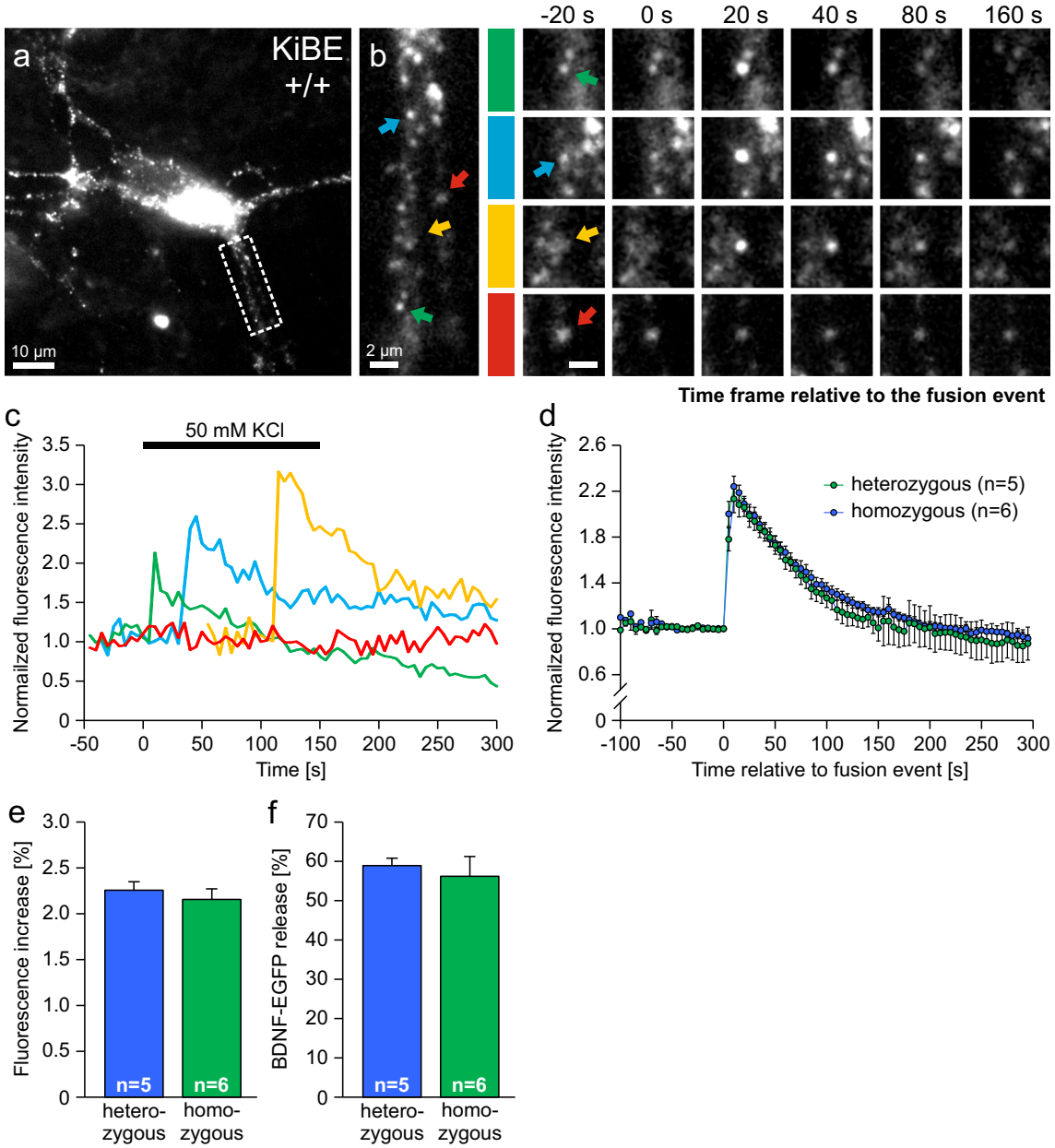

Fig. 10 Measurement of BDNF-GFP release from BDNF-GFP vesicles in dendrites of cultured hippocampal KiBE mouse neurons. **a** Live cell imaging of elevated K^+ (50 mM) depolarization-induced BDNF-GFP release from vesicles in cultured hippocampal neurons from KiBE mice, recorded at 14 DIV with epifluorescence microscopy. **b** White boxed ROI in (**a**) is shown at higher magnification (scale bar: 1.5 µm). Colored arrows and corresponding color coded magnified views on the right depict individual BDNF-GFP vesicles at different time points after start of the fusion event (at 20 s; time line of all fusion events was aligned to 0 s = last image before FPO). **c** Fluorescence traces of fusing (green, blue, yellow) or non-fusing vesicles (red) marked in (**b**) without aligning FPO of the vesicles. The sequential fusion events occur between 10 and 100 s after start of depolarization, indicating highly delayed FPO of *endogenous* BDNF-GFP vesicles. **d** Average decline in fluorescence intensity of single BDNF-GFP vesicles as shown in (**b**) ($KiBE^{+/-}$: 61 vesicles, $KiBE^{+/+}$: 69 vesicles). **e** Normalized fluorescence increase (due to pH neutralization) after FPO at 100–160 s after start of the depolarization ($KiBE^{+/-}$: 2.3 ± 0.1/$KiBE^{+/+}$: 2.2 ± 0.1; *t* test: $t = 0.65$, $p = 0.53$). **f** BDNF-GFP release amplitude as shown in (**d**) (fluorescence intensity at 20 s vs. 300 s). $KiBE^{+/-}$: 58.9 ± 1.9%; $KiBE^{+/+}$: 56.2 ± 5.0%; *t* test: $t = 0.58$, $p = 0.58$)

increase in fluorescence, nor the decay time course or the net release were significantly different between homozygous and heterozygous KiBE mouse neurons, respectively. The observed long delays for FPO (10–200 s; Fig. 9f) and the ongoing BDNF release at time points beyond 100 s after start of depolarization (Fig. 10d) suggest that BDNF secretion proceeds several orders of magnitude more slowly than neurotransmitter release.

These are the first live cell imaging measurements of a GFP-tagged neuropeptide in a knock-in mouse that synthetizes the neuropeptide at physiologically low levels. The results reveal that synaptic secretion even of the extraordinarily sparsely expressed neurotrophin BDNF can be monitored with high temporal and spatial resolution in a BDNF-GFP knock-in mouse.

Discussion

The dynamics of *endogenous* BDNF secretion from neurons has thus far remained elusive. We now addressed this question with a completely novel approach. We knocked in GFP-tagged BDNF (KiBE) into the endogenous mouse BDNF gene locus. The obtained KiBE mouse model allows to directly detect BDNF expression by intrinsic fluorescence without the need to use potentially artifact-prone immunocytochemical or other staining procedures. Moreover, BDNF-GFP expression in this mouse model is regulated by the *endogenous* BDNF gene regulatory elements, thereby excluding any potential artifacts that might be introduced when overexpressing BDNF-GFP.

KiBE mice survive well and do not show any obvious deficits, thus pointing to a largely intact secretion and biological function of BDNF-GFP in KiBE mice as compared to BDNF in wt animals. Also, protein expression levels and efficacy of cleavage of pro-BDNF-GFP to mBDNF-GFP in KiBE mice are not different from untagged BDNF in wt mice (see Fig. 1).

Using confocal and STED super resolution microscopy in KiBE mice allowed us to assign *endogenous* BDNF-GFP vesicles in neuronal processes of hippocampal neurons predominantly to dendrites, whereas axonal targeting was less prominent. Accordingly, BDNF-GFP vesicles were frequently observed close to postsynaptic structures. Live cell imaging of BDNF-GFP vesicles in KiBE mouse hippocampal neurons allowed us for the first time to visualize release of the low levels of *endogenous* BDNF in living cells under in all aspects physiological conditions. These results unambiguously pinpoint a prominent dendritic localization of *endogenous* BDNF and clearly rule out an exclusive axonal expression of BDNF that has previously been much emphasized by one study [27].

Absence of BDNF ko Phenotype

Homozygous BDNF ko mice were reported to die mostly within the first week after birth due to severe sensory neuron dysfunctions leading to obvious problems with breathing, cardiac function, body weight, and movement abnormalities [28–30], and survive only in extremely rare cases until puberty. In contrast, heterozygous BDNF ko mice ($BDNF^{+/-}$) do not show any lethal malfunctions but rather develop impaired synaptic plasticity that seems to underlie deficits in memory formation, cognitive functions, and altered social behavior in these mice (see e.g., [30–33]). Since homozygous KiBE mice ($KiBE^{+/+}$) survive until old ages without any signs of the above mentioned live threatening dysfunctions (Suppl. Fig. 1), we conclude that BDNF-GFP retains by large the biological function of wt BDNF in the KiBE animals. This is in line with our previous report that BDNF-GFP released from HEK293 cells supports TrkB signaling with similar efficacy as wt BDNF [6]. This is also consistent with our observation in the present study that the levels of pro-BDNF-GFP and the efficacy of pro-BDNF-GFP processing to mBDNF-GFP are, both, indistinguishable from the respective results for wt BDNF (Fig. 1). This intact processing of BDNF-GFP is important to assure a physiological balance between the partially counteracting pro-BDNF-GFP/$p75^{NTR}$ and mBDNF-GFP/TrkB signaling pathways. Nevertheless, future additional studies will be required to resolve the complete spectrum of the KiBE mouse phenotype.

Distribution of BDNF-GFP in Hippocampus Is Identical to *Endogenous* BDNF

Expression of wt BDNF was reported previously to be confined to specific subsets of cells in the brain and this expression pattern can be explained by the (in part activity-dependent) tight regulation of BDNF expression by the specific promoter elements controlling the transcription of untranslated upstream exons 1–8 [20]. For example, wt BDNF mRNA and protein are expressed in many types of glutamatergic neurons throughout the brain but are under physiological conditions not found in GABAergic or other types of inhibitory interneurons (see e.g., [34, 35]). Rather, development of interneurons depends on BDNF supply provided by synaptic contacts of inhibitory neuron presynaptic terminals onto glutamatergic neurons [36]. Moreover, while this is still a matter of debate, astrocytes or other glial cells were reported to lack de novo BDNF synthesis under physiological conditions, although re-use for exocytosis of previously endocytosed BDNF by glial cells has been suggested (reviewed by [10, 35]). Our results in KiBE mice provide strong evidence that the above mentioned cellular expression pattern of wt BDNF

is completely retained for BDNF-GFP. Like for wt BDNF, we observe within the hippocampus the strongest BDNF-GFP expression (meaning both, incidence of expressing cells and signal strength per cell) in CA3 pyramidal neurons, followed by dentate gyrus granule cells, and CA1 pyramidal neurons (see Fig. 2 and Suppl. Fig.2). Apart from these cell layers, only selected cell bodies in the hilar region (i.e., CA4) are strongly positive for BDNF-GFP, while there was no indication of BDNF-GFP expression in GABAergic interneurons in stratum radiatum and/or stratum oriens in KiBE mice. This cell-specific expression of BDNF-GFP in the hippocampus of KiBE mice is in line with previous results obtained with different BDNF antibodies (see e.g., [14, 16, 17]).

Subcellular Targeting of BDNF-GFP

It could be argued that attaching the 29 kD C-terminal GFP tag to the 32 kD pre-pro-BDNF sequence might interfere with targeting of the protein in neurons and, specifically, with the subcellular targeting to axons and the somato-dendritic region. Previous studies addressing the colocalization of BDNF-GFP with numerous subcellular markers speak against a general mistargeting but rather identified the presence of BDNF-GFP selectively in cellular compartments that are typical for the transit of secreted proteins [6, 19]. Also, these previous studies suggested axonal as well as dendritic targeting of overexpressed BDNF-GFP (see e.g., [8, 9, 19]), but also for wt BDNF (see e.g., [37–39], reviewed in [3]). Our results in KiBE mice stress the combined axonal and dendritic targeting of BDNF-GFP vesicles also in the absence of overexpression. In cultures of postnatal hippocampal neurons from KiBE mice, dendritic expression (~ 70%; compare Fig. 6) seems to be more prominent than targeting to axons (~ 30%). Accordingly, we observed in acute and in fixed hippocampal slices BDNF-GFP vesicles in primary dendrites of CA1 and CA3 pyramidal neurons as well as in granule cell dendrites of the dentate gyrus (Figs. 2, 3, and 4). These results clearly establish dendritic targeting of *endogenous* BDNF-GFP vesicles in all hippocampal principle neurons. Nevertheless, due to the extremely low expression of BDNF under physiological conditions and the resulting dim fluorescence of BDNF-GFP vesicles in KiBE mice, the presence of BDNF-GFP vesicles in thin distal dendrites and also in axons of KiBE mouse neurons in hippocampal slices cannot be excluded.

Targeting of BDNF-GFP to Synaptic Structures

The colocalization analysis with the presynaptic marker protein Bassoon (Fig. 8) and the postsynaptic marker protein PSD95 (Fig. 7) is overall consistent with presynaptic as well as postsynaptic localization of BDNF-GFP vesicles in KiBE mice. However, together with the more prominent dendritic (i.e., 70%) than axonal (30%) localization of BDNF-GFP vesicles in hippocampal slices and cultured neurons of KiBE mice (Figs. 3, 4, 5, and 6), these data establish postsynaptic targeting and secretion as an important feature of *endogenous* BDNF in the brain. This is in line with prominent dendritic and postsynaptic secretion of *endogenous* BDNF-GFP in cultured KiBE mouse neurons (Figs. 9 and 10, Suppl. Fig.5). The nearest neighbor analysis of STED imaged BDNF-GFP vesicles relative to Bassoon and PSD95, respectively, does not allow assigning an exclusive pre- or postsynaptic localization to BDNF vesicles (Figs. 7 and 8; Suppl. Fig.4). Interpretation of these results needs to take into account that—unlike transmitter vesicles—BDNF-GFP secretory granules are not accumulated directly underneath pre- or postsynaptic membranes, like PSD95 and Bassoon. At glutamatergic synapses, the average distance between postsynaptic PSD95 and presynaptic Bassoon is ~ 100 nm (see e.g., [40, 41]) whereas BDNF-GFP vesicles can be found up to 1 μm away from Bassoon or PSD95, respectively (Suppl. Fig. 4). Only ~ 10% of BDNF-GFP vesicles are found within a perimeter of 100 nm around the pre- or the postsynaptic marker, respectively, and can thereby be judged to be close to the pre- or postsynaptic membrane. However, the majority of BDNF-GFP vesicles is located 100–1000 nm away from Bassoon and could be present in apposed postsynaptic spines, like the ones being 100–1000 nm away from PSD95 could be present in the corresponding presynaptic terminal.

Taken together, our colocalization analysis suggests pre- and postsynaptic localization of *endogenous* BDNF vesicles in KiBE mouse hippocampal neurons, being consistent with the localization of ~ 70% of BDNF-GFP vesicles in dendrites and 30% of BDNF-GFP vesicles being present in axons. These results are in line with axonal [27] as well as parallel axonal and dendritic targeting [18] of *endogenous* BDNF in EM sections of hippocampal slices. It remains to be determined whether the quantitative differences in presynaptic vs. postsynaptic targeting observed in our and in these two previous studies result from distinct sensitivities of the three detection methods towards axonal and dendritic BDNF vesicles, respectively, or from differences in the biological status of the mice prior to slice preparation [39, 42, 43].

Properties of BDNF-GFP Vesicles and Release

This is the first study that visualizes with live cell imaging the release of *endogenous* BDNF (Figs. 9 and 10). Theoretical considerations suggested that the GFP tag on BDNF might slow down diffusion of BDNF-GFP by a factor of 1.8 compared to wt BDNF [6]. Nonetheless, the GFP tag does apparently not interfere with the release of sufficient quantities of biologically active BDNF-GFP in vivo, as is obvious from the healthy maturation of homozygous KiBE mice ($KiBE^{+/+}$)

compared to early postnatal death of homozygous BDNF ko mice (see e.g., [28]). Whether the kinetics and amplitudes of BDNF-GFP release are identical to BDNF without GFP tag can for obvious reasons not be answered, since wt BDNF cannot be detected with live cell imaging. Therefore, our release results for BDNF-GFP in KiBE mice can only be compared to data obtained with overexpressed BDNF-GFP, or between heterozygous ($KiBE^{+/-}$) and homozygous ($KiBE^{+/+}$) KiBE mice (Figs. 9 and 10, Suppl. Fig.5). We observed that probability, dilation, and kinetics of fusion pore openings, as well as the time course and magnitude of release are indistinguishable between $KiBE^{+/-}$ and $KiBE^{+/+}$ animals. Likewise, the release properties of both genotypes cannot be distinguished from properties of overexpressed BDNF-GFP in wt mouse neurons. Interestingly, the average fluorescence intensity of BDNF-GFP vesicles in $KiBE^{+/-}$ animals matches exactly 50% of the value recorded in $KiBE^{+/+}$ neurons (see Suppl. Fig. 5). This suggests that wt BDNF and BDNF-GFP are targeted together into the same vesicles and compete for the available space therein. Alternatively, the reduced fluorescence in $KiBE^{+/-}$ neuron vesicles might indicate that loading of individual BDNF-GFP granules is controlled by the expression level of the peptide, which is lower in $KiBE^{+/-}$ neurons compared to BE overexpressing cells, but also lower than in $KiBE^{+/+}$ neurons.

To our knowledge, we describe here for the first time the direct visualization of neuropeptide secretion from single vesicles using a knock-in approach with fully retained transcriptional regulation of the endogenous gene locus. This strategy has not been used for any other neuropeptide before, and our study is a proof of concept for analyzing secretion of endogenous neuropeptides with a GFP knock-in. We selected BDNF-GFP for this approach because the release of BDNF in the CNS is key to understanding cellular mechanisms regulating learning and memory as well as neurological and neurodegenerative diseases ranging from major depression and dementia, over Huntington's disease and autism to schizophrenia [44–48]. We think that this mouse model will enable to unambiguously answer many long-standing and so far controversially debated questions where, when, and to what extent *endogenous* BDNF is expressed, transported, and released in the brain—under physiological conditions as well as in case of disease.

Materials and Methods

Targeting Strategy and Generation of KiBE Mice

To generate the targeting vector harboring the two homology arms of the mouse BDNF gene (NCBI RefSeq ID: NW_001030694.1), the BAC clone RP23-390F19 (Bacpac Resources Center Children Hospital, Oakland Research Institute, CA) was used. In the first cloning step, a polymerase chain reaction (PCR) was performed to amplify the left homology arm with part of the BDNF coding sequence yielding a 2.5-kb fragment comprising the 5′ EcoRV restriction site outside and the 3′ XmaI site inside the coding sequence. This fragment was then cloned into the pBluescript vector KSII- (Stratagene) via EcoRV and XmaI. An overlap PCR was performed first with primers to amplify a 1.25-kb fragment from the Clontech vector pEGFP N1 harboring the coding sequence of mouse pre-pro-BDNF-eGFP [6, 21] generating overlaps to the right homology arm and comprising the XmaI site inside the BDNF coding sequence. When using the BAC clone as template DNA in a second PCR, a 5′ overlap to GFP sequence was produced obtaining a 4.9-kb fragment which contained the respective XbaI site in the right homology arm (see targeting construct scheme, Fig. 1a). Both obtained DNA fragments served then as template for a third PCR reaction with both outside primers to generate a 6.15-kb long fragment, which was then subcloned via XmaI and XbaI into the pBluescript KSII vector, which contained already the left homology arm and the 5′ part of the BDNF coding sequence. Furthermore, a frt-flanked PGK neomycin resistance cassette (from pSVaZ11-PGK-Neo vector) for positive ES cell selection was introduced 5′ to the BDNF-GFP sequence. In addition, to guarantee negative selection in ES cells with ganciclovir, a HSV-TK cassette (MC1 TK) was subcloned 5′ to the frt-flanked PGK neomycin resistance cassette. The targeting vector was constructed to achieve that a BglII digest could serve for the subsequent analysis of ES cell clones and founder mice by Southern blotting. Linearization of the targeting construct for electroporation into ES cells (C57BL/6) was achieved by NotI digestion. The targeting vector was completely sequenced to ensure the functional integrity of the construct. Southern blotting of selected ES cell clones was performed as described previously [49] after BglII restriction digest of genomic DNA. Hybridization probes were generated by PCR with appropriate DNA templates and the following primer pairs: 5′probe fw: 5′-AGCAAATGGCTGTCATGGAG-3′, 5′ probe rev: 5′-AGCCTCATTCCTTCTGTCC-3′; 3′probe fw: 5′-ATCTATTTATGTGGCATGAC C-3′, 3′probe rev: 5′-CTTCAGACACATCCTGTCAT-3′; Neo probe fw: 5′-TGCTCGACGTTGTCACTGAAGC-3′ and Neo probe rev: 5′-TACCGTAAAGCACGAGGAAGC-3′. Recombined ES cell clones were injected into blastocysts yielding chimeric animals which were then crossbred with wt C57BL/6J animals to yield germline transmission. Animals of the F1 generation containing the knock-in construct were crossbred with flipase-deleter mice [50], carrying the germline expression of the recombinase flipase in order to delete the frt-PGK-Neo selection cassette.

Generation of recombinant ES cells, blastocyst injection, and production of founder animals were performed by Genoway, Lyon, France.

Genotyping of KiBE Mice

Genotyping was performed by PCR from tail genomic DNA using three different primers in a single PCR reaction (1 × 94 °C 3 min; 30 × 94 °C 30 s/61 °C 45 s/72 °C 45 s; and 1 × 72 °C 3 min). A wild-type band of 532 bp was detected by the BDNF-forward primer (BDNF fw2: 5′-GGGA GCTGAGCGTGTGTGACAGTA-3′) and a reverse primer, located in the 3′ untranslated region of the BDNF gene (3UTR rev: 5′-TCCTTTCAGGTCATGGGATATGTCC-3′). In case of presence of the knock-in allele, a fragment of 621 bp was obtained by use of the reverse primer detecting GFP sequences (GFP rev: 5′-ATGGCGGACTTGAA GAAGTCGTG-3′). In case of presence of the Ki allele, a fragment of 621 bp was yielded by usage of the reverse primer against GFP sequence (GFP rev: 5′-ATGGCGGACTTGAA GAAGTCGTG-3′).

Breeding Scheme and Keeping of Animals

All experiments were performed with homozygous, heterozygous, and wild-type littermates derived from heterozygous KiBE (KiBE$^{+/-}$) breeding pairs that had been backcrossed for more than 10 generations with C57BL/6J mice (JAX mice, Charles River, Sulzfeld, Germany). Animals (all three genotypes together) aged 1 to 18 months were housed in groups of 2 to 4 animals per cage. Mice were kept on a 12:12 h circadian rhythm (light onset at 7 am). They had access to food and water ad libitum. Cages were equipped with enriched environment (running wheel with cot; tunnels and different toys) and nesting material. Experiments were conducted in accordance with the guidelines for the use of animals (Directive 2010/63/EU).

Homozygous BDNF knockouts used for control lysates were obtained by breeding of heterozygous BDNF knockout animals [30] and were used at postnatal day 2.

Hippocampal Microcultures

Microcultures were prepared as described previously [51]. Primary cortical astrocytes from P0-P3 Sprague-Dawley rats were isolated and cultured for 2–3 weeks in BME medium supplied with 10% FCS. After confluence was reached, astrocytes were split and seeded on glass coverslips at a density of 50,000 cells and cultured in a 3.5-cm culture dish. At DIV 3, proliferation was inhibited by adding 3–5 μM AraC to the medium. After 2–3 weeks, hippocampal neurons of KiBE$^{+/+}$, KiBE$^{+/-}$ mice, or their wt littermates were isolated from P0–P2 mice and seeded onto the astrocyte islands. Neurons were enabled to attach to astrocytes before the culture medium was replaced by Neurobasal medium containing 2% B27 supplement. Microcultures were used for live cell imaging 11–14 days after plating of neurons.

Transfection of Cultured wt Neurons

Hippocampal neurons from wt mice were transfected at DIV 6–8 with the respective plasmids using calcium phosphate precipitation [19]. In brief, up to 4.5 μg plasmid DNA per 3.5 cm culture dish was used to form precipitates in the presence of 10 mM $CaCl_2$ in BES buffer. Cells were incubated in NB/B27 containing the transfection mix for 2.5 h in the presence of 10 μM DNQX and 100 μM D,L-AP5. Conditioned medium was reapplied after washing the cells in PBS. Neurons were used for imaging experiments 5 days after transfection (DIV 11–14).

Preparation of Hippocampal Slices for IHC

Coronal slices were prepared from young adult male and female KiBE$^{+/-}$, KiBE$^{+/+}$, or wt littermates at an age of 3–4 months. Animals were anesthetized using isoflurane and decapitated. After opening, the cranium brains were quickly removed and placed in ice-cold ACSF solution. Brains were cut to 350 μm thick acute coronal or transversal brain slices using a vibratome (Leica VT 1200 S). Slices containing the hippocampus were selected, fixed in 4% PFA for 1 h and incubated in 30% sucrose over night at 4 °C. Slices were then cryosectioned to 40 μm thick slices using a microtome (Leica) and either processed for antibody stainings or kept unstained. For imaging experiments, slices were transferred to slides (Superfrost) and imaged without mounting using a 63× water immersion objective.

Western Blotting

Lysates of brain tissue were prepared from 4- to 8-week-old KiBE animals and from postnatal day 2 animals in case of homozygous BDNF knockouts. Preparation of lysates, SDS-acrylamide gel electrophoresis, and Western blotting was performed as previously described [52]. The following primary antibodies were used: rabbit anti-BDNF (Abcam) 1:3000, mouse anti-GFP 1:500 (Roche), and mouse anti-tubulin 1:5000 (Sigma). Signal detection was achieved by ECL Prime Western blotting detection reagent (GE healthcare) and the Peqlab FUSION-SL Advance 4.2 MP analyzer. Quantification was performed by densitometric analysis using the Bio1D 15.02 software (Vilber Lourmat).

Immunocytochemistry/Immunohistochemistry

Staining procedures were performed on cultured hippocampal neurons at 7–14 DIV, or on coronal hippocampal slices. Hippocampal neuron cultures or slices were fixed in the presence of 4% PFA in PBS and permeabilized with 0.1% TritonX. Cells were stained with primary antibodies over night at 4 °C. Primary antibodies were mouse anti-MAP2

(1:1000, MAB3418, Merck Chemicals, UK), mouse anti-SMI 312 (1:1000, Synaptic Systems), mouse antiPSD95 (1:300, Thermo Scientific), chicken anti-GFP (1:400, 1020, Aves) for slices, and rabbit anti-GFP polyclonal serum (1:3300, kindly provided by Dr. Matthias Klugmann, Sydney) for primary neurons. Secondary antibodies conjugated with Alexa Fluor 488 (1:1000), Alexa Fluor 568 (1:1000), and Alexa Fluor 633 (1:1000) (Life technologies, Carlsbad, CA) were incubated at room temperature for 2 h. For STED experiments, Atto 594 anti-mouse (1:200, Sigma-Aldrich) and Atto 647N anti-rabbit (1:200, Sigma-Aldrich) conjugated secondary antibodies were used. Colocalization studies were performed using a confocal imaging system (LSM 780, Zeiss, Germany) attached to an upright fluorescence microscope (Axio examiner Z1, Zeiss, Germany) equipped with 20× and 60× water immersion objective (NA: both 1.0, Zeiss, Germany). Green fluorescence was excited using 488 nm laser line from an Argon laser and red or infrared fluorescence was excited using 543 nm or 633 nm laser lines from a Helium/Neon laser. Signals were detected by a photon multiplier using a GaAsP-detector array or PMT detectors.

Immunoperoxidase labeling was performed as described previously [53]. Free-floating formaldehyde-fixed sections were treated with 50% methanol and 1% H2O2 in PBS for 20 min, washed in PBS, incubated in a solution containing 10% normal goat serum (NGS) and 0.3% Triton X-100 for 60 min followed by the anti-GFP antibody (Invitrogen, 1:2000) solution supplemented with 0.1% sodium azide for 72 h at 6 °C. After washing and incubation in PBS containing 0.2% bovine serum albumin (PBS-A, 1h), sections were incubated with biotinylated secondary goat-anti-rabbit antibody (Vector, 1:2000 in PBS-A) for 20 h at RT. After washing, sections were incubated for 4 h with ABC complex (Vector Elite ABC kit, 1:1000) in PBS-A, followed by incubation with peroxidase substrate solution (1.4 mM 3,3′-diaminobenzidine tetrahydrochloride DAB, 0.015% H_2O_2 in Tris/HCl buffer) for 4 min.

Linear Unmixing

Due to the low fluorescence intensity of *endogenous* BDNF-GFP compared to background fluorescence in hippocampal slices, the linear unmixing feature of the Zeiss LSM 780 operated by the ZEN software was employed. This procedure enabled us to separate the unique turquoise part of the GFP spectrum (wavelength range: 505–520 nm) from a strong background fluorescence when using the 488 nm line of the Argon laser for excitation. For linear unmixing, the 32-channel GaAsP detector of the Zeiss LSM 780 was used. Linear unmixing was performed on λ-stacks (usually 11 slices separated by 1 μm) using reference spectra extracted from λ-coded reference images (specific green-turquoise GFP spectra obtained from unstained homozygous KiBE slices, red Alexa 568 spectra obtained from stained wt slices, unspecific green-yellow background spectra obtained from unstained wt slices). The portion of the green fluorescence that was assigned by the ZEN software algorithm exclusively to GFP is shown as green fluorescence in all pictures processed with the linear unmixing procedure.

STED Imaging

Stained cultured hippocampal neurons of $KiBE^{+/+}$ or wt littermates were imaged using a Leica TSC SP8 STED 3× microscope equipped with a 63× oil immersion objective (NA = 1.4, Leica) for confocal and a 100× oil immersion objective (NA = 1.4, Leica) for STED imaging. Fluorescence of the antibody staining was excited using a white light laser at wavelengths of 580 and 650 nm under simultaneous depletion of fluorescence using a 775-nm pulsed STED laser source. Images were acquired using LasX software (Leica) as z-stacks (100 nm/plane) with an xy resolution of about 40 nm. Deconvolution of z-stack data was performed using Huygens Professional software (Scientific Volume Imaging). Deconvolved images were analyzed in 3D using Imaris (Bitplane) and processed for top view (xy) and orthogonal projections (xz).

Quantification of Dendritic Localization

Using adapted ImageJ macros, z-stacks of anti-MAP2 STED images of a cell (excluding the soma) were collapsed into one image plane and defined as the 2-dimensional representation of the dendritic area of a cell. Z-stacks of BDNF-GFP vesicles of the same cell were combined in the same way into one plane and thresholded using 2× the standard deviation of green background fluorescence. Colocalization analysis of both images was performed and quantified as the percentage of BDNF-GFP fluorescence coinciding with MAP2 (ImageJ macro).

Quantification of Proximity Between Synaptic Markers and BDNF-GFP Vesicles

For nearest neighbor analysis of PSD95 and BDNF-GFP structures, z-stacked STED images of PSD95 were combined as described above into one image plane, using ImageJ macros. Neuritic structures of a cell were defined by ROIs, in which PSD95 particles were detected by thresholding. Z-Stacks of BDNF-GFP vesicles of the same cells were thresholded and detected (compare above) within the same ROIs defined for PSD95. For nearest neighbor analysis, the number of PSD95 particles (reference point: center of mass) within a certain distance (bin size: 20 nm) to the center of mass of BDNF-GFP particles of the same cell was calculated and plotted in a histogram (Suppl. Fig. 4). An identical procedure

was used to quantify the average distance between Bassoon particles and BDNF-GFP particles in other cells.

Preparation and Recording of Acute Hippocampal Slices for Live Cell Imaging Ex Vivo

Transversal slices were prepared from young adult male and female KiBE$^{+/-}$, KiBE$^{+/+}$, or wt littermates at an age of 8–16 weeks. Animals were anesthetized using isoflurane. After cervical dislocation, brains were quickly removed in ice-cold ACSF of the following composition (in mM): NaCl, 125; KCl, 3; $NaHCO_3$, 25; NaH_2PO_4, 1.25; CaCl2, 2.5; $MgCl_2$, 1.5; Glucose, 10; equilibrated with 5%CO_2/95%O_2 to a pH of 7.35. Hippocampal slices were prepared as transversal sections (thickness: 350 μm) on a vibratome (Model 1000, The Vibratome Company, St. Louis, USA), and kept submerged first for 30 min at 33 °C and subsequently at room temperature. For live cell imaging, slices were transferred to an experimental chamber mounted on the stage of the LSM 780 and constantly superfused with fresh ACSF at room temperature.

Live Cell Imaging/Fluorescence Microscopy of Cultured Neurons

Coverslips containing KiBE or WT neurons were transferred into a bath chamber (Luigs & Neumann, Germany) filled with HEPES (20 mM HEPES, 100 mM NaCl, 4 mM KCl, 1 mM Na_2HPO_4, 2 mM $CaCl_2$, 1 mM $MgCl_2$, 100 μM Glycine) and inspected with a fluorescence microscope (BX51W, Olympus, Melville, NY) using a 60× water immersion objective (LUMFI, NA 1.1, Olympus, Melville, NY). Wavelength selection was accomplished by using filter sets (Chroma Techn. Corp.) for green (excitation: 470 ± 20 nm, emission: 525 ± 25 nm) and red (excitation: 572 ± 17.5 nm, emission: 632 ± 30 nm) fluorescence mounted on filter wheels. Image capture was performed using a CCD camera (CoolSnap HQ^2, 14bit dynamic range, PhotoMetrics, Huntington Beach, CA) controlled by VisiView software (Visitron Systems, Germany). Unless otherwise specified, the exposure times for recordings (between 0.3 and 1.5 s) were adjusted for every cell. Image acquisition rates ranged from 0.3 to 0.1 Hz [6].

BDNF-GFP Release and Related Assays

KiBE mouse neurons or wt neurons transfected with plasmids driving expression of BDNF-GFP were prepared for live cell imaging of activity-dependent fusion pore opening (FPO) and BDNF-GFP cargo release. The magnitude and time course of FPO and cargo release from BDNF-GFP vesicles is not different between elevated potassium (50 mM K^+)-induced depolarization and action potential stimulation [54]. Nevertheless, to evenly stimulate release events throughout the field of view, we used the elevated potassium stimulation here. After recording baseline fluorescence levels, BDNF-GFP release was stimulated by applying HEPES buffer containing 50 mM KCl (adjusted for equal osmolarity) to a single recorded cell by a local perfusion system [8]. The superfusion system consisted of a multi-barreled application pipette containing control and depolarizing solutions with a common outlet and an opposed drain pipette creating a laminar flow of solution [55]. The superfusion system was positioned at a distance of ~400 μm from the recorded cell allowing complete exchange of applied solutions within 10 s [21]. Using this superfusion system, we observed similar delays, kinetics, and time courses of BDNF-GFP secretion as described previously for depolarization induced and electrically induced BDNF release in hippocampal neurons [8, 13, 26]. At the end of a measurement, HEPES buffer containing 0.3 mM BPB was superfused to discriminate content release from re-acidification. Negative controls were obtained by analyzing closed BDNF-containing granules showing no change in fluorescence intensity throughout the recording. Kinetics of vesicle fusion events were measured by applying HEPES buffer containing 50 mM KCl in the presence of 0.3 mM BPB. Single vesicle fusion events were observed by immediate quenching of GFP fluorescence after fusion pore opening [21]. Either dendritic regions containing vesicle clusters (3–15 vesicles) or single vesicles were analyzed for each measurement.

Image Processing

Image analysis was performed using MetaMorph software (Universal imaging Corporation, West Chester, PA). Between 8 and 20 regions of interest (single vesicles/dendritic branches) were selected to cover the average change in fluorescence intensity of a single cell. Background fluorescence intensities were subtracted for each region and the average intensity was normalized to the time point before stimulation/treatment. A mono-exponential extrapolation of the photobleaching observed during baseline recordings was applied to correct the normalized fluorescence data [6]. Single cell fluorescence data were averaged to obtain the mean fluorescence intensity changes (BDNF-GFP release and related assays, live cell pH titration).

Statistical Analysis

Statistical analysis was performed by using GraphPad Prism (GraphPad Software Inc., La Jolla CA, USA) software. Experiments were analyzed either by two-sided *t* test comparisons or in case of multiple comparisons by one-way ANOVA (analysis of variances). All data were checked for normal distribution by using Shapiro-Wilk test. If not otherwise indicated, all data followed the normal distribution. Statistical

significance was determined as $p < 0.05$. The sample size was calculated with G-Power (University of Düsseldorf, Germany) based on our previous experience with BDNF-GFP vesicle properties. In the release experiments, a total sample size of 10 was calculated given a significance level (alpha) of 0.05, and a power of 0.8. All data are depicted as mean ± standard error of the mean (SEM).

Reagents

AraC, bromphenol blue, $CaCl_2$, glucose, glycine, KCl, NH_4Cl (Sigma, St. Louis, MO); B27, DNQX, DL-AP5 (Tocris Bioscience, UK); Bafilomycin A1 (Merck Chemicals, UK); BME, FCS, NB, Nigericin, PBS, (Life technologies, Carlsbad, CA); pEGFP-N1 (CloneTech, Palo Alto, CA).

Acknowledgements We would like to thank Dr. Kurt Gottmann for valuable suggestions and discussions, Sabine Eichler, Regina Ziegler, Margit Schmidt, Anja Reupsch, Danka Dormann, Andrea Conrad, Anisa Kosan, and Ruth Jelinek, for expert technical assistance, Yury Kovalchuk for valuable suggestions regarding the linear unmixing procedure, as well as Ralf Mohrmann for important comments on the manuscript.

Author Contributions Experiments were performed by JL, RE, TB, TM, KR, EE. The data were analyzed by RE, JL, TE, TM, TB, EE, OK, WZ and VL. Experiments were designed by VL, BL, TB, JL. The study was designed and supervised by VL and BL. The manuscript was written by VL with the help of BL, JL, TB, TE, TM.

Funding This work was funded by the German Research foundation (DFG SFB 779 and LE 1020/2-1 to VL, and LU 775/5-1 to BL). The funders had no role in study design, data collection and analysis, decision to publish, or preparation of the manuscript.

Compliance with Ethical Standards

Conflict of Interest The authors declare that they have no conflict of interest.

References

1. Bramham CR, Messaoudi E (2005) BDNF function in adult synaptic plasticity: the synaptic consolidation hypothesis. Prog Neurobiol 76(2):99–125. https://doi.org/10.1016/j.pneurobio.2005.06.003
2. Cowansage KK, LeDoux JE, Monfils MH (2010) Brain-derived neurotrophic factor: a dynamic gatekeeper of neural plasticity. Curr Mol Pharmacol 3(1):12–29
3. Edelmann E, Lessmann V, Brigadski T (2014) Pre- and postsynaptic twists in BDNF secretion and action in synaptic plasticity. Neuropharmacology 76(Pt C):610–627. https://doi.org/10.1016/j.neuropharm.2013.05.043
4. Gottmann K, Mittmann T, Lessmann V (2009) BDNF signaling in the formation, maturation and plasticity of glutamatergic and GABAergic synapses. Exp Brain Res 199(3–4):203–234. https://doi.org/10.1007/s00221-009-1994-z
5. Park H, Poo MM (2013) Neurotrophin regulation of neural circuit development and function. Nat Rev Neurosci 14(1):7–23. https://doi.org/10.1038/nrn3379
6. Brigadski T, Hartmann M, Lessmann V (2005) Differential vesicular targeting and time course of synaptic secretion of the mammalian neurotrophins. J Neurosci 25(33):7601–7614. https://doi.org/10.1523/JNEUROSCI.1776-05.2005
7. Dean C, Liu H, Dunning FM, Chang PY, Jackson MB, Chapman ER (2009) Synaptotagmin-IV modulates synaptic function and long-term potentiation by regulating BDNF release. Nat Neurosci 12(6):767–776. https://doi.org/10.1038/nn.2315
8. Hartmann M, Heumann R, Lessmann V (2001) Synaptic secretion of BDNF after high-frequency stimulation of glutamatergic synapses. EMBO J 20(21):5887–5897. https://doi.org/10.1093/emboj/20.21.5887
9. Kohara K, Kitamura A, Morishima M, Tsumoto T (2001) Activity-dependent transfer of brain-derived neurotrophic factor to postsynaptic neurons. Science 291(5512):2419–2423. https://doi.org/10.1126/science.1057415
10. Lessmann V, Gottmann K, Malcangio M (2003) Neurotrophin secretion: current facts and future prospects. Prog Neurobiol 69(5):341–374
11. Matsuda N, Lu H, Fukata Y, Noritake J, Gao H, Mukherjee S, Nemoto T, Fukata M et al (2009) Differential activity-dependent secretion of brain-derived neurotrophic factor from axon and dendrite. J Neurosci 29(45):14185–14198. https://doi.org/10.1523/JNEUROSCI.1863-09.2009
12. Kojima M, Takei N, Numakawa T, Ishikawa Y, Suzuki S, Matsumoto T, Katoh-Semba R, Nawa H et al (2001) Biological characterization and optical imaging of brain-derived neurotrophic factor-green fluorescent protein suggest an activity-dependent local release of brain-derived neurotrophic factor in neurites of cultured hippocampal neurons. J Neurosci Res 64(1):1–10. https://doi.org/10.1002/jnr.1080
13. Edelmann E, Cepeda-Prado E, Franck M, Lichtenecker P, Brigadski T, Lessmann V (2015) Theta burst firing recruits BDNF release and signaling in postsynaptic CA1 neurons in spike-timing-dependent LTP. Neuron 86(4):1041–1054. https://doi.org/10.1016/j.neuron.2015.04.007
14. Conner JM, Lauterborn JC, Yan Q, Gall CM, Varon S (1997) Distribution of brain-derived neurotrophic factor (BDNF) protein and mRNA in the normal adult rat CNS: evidence for anterograde axonal transport. J Neurosci 17(7):2295–2313
15. Wetmore C, Cao YH, Pettersson RF, Olson L (1991) Brain-derived neurotrophic factor: subcellular compartmentalization and interneuronal transfer as visualized with anti-peptide antibodies. Proc Natl Acad Sci U S A 88(21):9843–9847
16. Wetmore C, Olson L, Bean AJ (1994) Regulation of brain-derived neurotrophic factor (BDNF) expression and release from hippocampal neurons is mediated by non-NMDA type glutamate receptors. J Neurosci 14(3 Pt 2):1688–1700
17. Yan Q, Rosenfeld RD, Matheson CR, Hawkins N, Lopez OT, Bennett L, Welcher AA (1997) Expression of brain-derived neurotrophic factor protein in the adult rat central nervous system. Neuroscience 78(2):431–448
18. Harward SC, Hedrick NG, Hall CE, Parra-Bueno P, Milner TA, Pan E, Laviv T, Hempstead BL et al (2016) Autocrine BDNF-TrkB signalling within a single dendritic spine. Nature 538(7623):99–103. https://doi.org/10.1038/nature19766
19. Haubensak W, Narz F, Heumann R, Lessmann V (1998) BDNF-GFP containing secretory granules are localized in the vicinity of synaptic junctions of cultured cortical neurons. J Cell Sci 111(Pt 11):1483–1493
20. Aid T, Kazantseva A, Piirsoo M, Palm K, Timmusk T (2007) Mouse and rat BDNF gene structure and expression revisited. J Neurosci Res 85(3):525–535. https://doi.org/10.1002/jnr.21139

21. Kolarow R, Brigadski T, Lessmann V (2007) Postsynaptic secretion of BDNF and NT-3 from hippocampal neurons depends on calcium calmodulin kinase II signaling and proceeds via delayed fusion pore opening. J Neurosci 27(39):10350–10364. https://doi.org/10.1523/JNEUROSCI.0692-07.2007
22. Matsumoto T, Rauskolb S, Polack M, Klose J, Kolbeck R, Korte M, Barde YA (2008) Biosynthesis and processing of endogenous BDNF: CNS neurons store and secrete BDNF, not pro-BDNF. Nat Neurosci 11(2):131–133. https://doi.org/10.1038/nn2038
23. Gibon J, Barker PA (2017) Neurotrophins and proneurotrophins. Neuroscientist 23(6):587–604 1073858417697037. https://doi.org/10.1177/1073858417697037
24. Lessmann V, Brigadski T (2009) Mechanisms, locations, and kinetics of synaptic BDNF secretion: an update. Neurosci Res 65(1):11–22. https://doi.org/10.1016/j.neures.2009.06.004
25. Shimojo M, Courchet J, Pieraut S, Torabi-Rander N, Sando R 3rd, Polleux F, Maximov A (2015) SNAREs controlling vesicular release of BDNF and development of callosal axons. Cell Rep 11(7):1054–1066. https://doi.org/10.1016/j.celrep.2015.04.032
26. Eckenstaler R, Lessmann V, Brigadski T (2016) CAPS1 effects on intragranular pH and regulation of BDNF release from secretory granules in hippocampal neurons. J Cell Sci 129(7):1378–1390. https://doi.org/10.1242/jcs.178251
27. Dieni S, Matsumoto T, Dekkers M, Rauskolb S, Ionescu MS, Deogracias R, Gundelfinger ED, Kojima M et al (2012) BDNF and its pro-peptide are stored in presynaptic dense core vesicles in brain neurons. J Cell Biol 196(6):775–788. https://doi.org/10.1083/jcb.201201038
28. Ernfors P, Lee KF, Jaenisch R (1994) Mice lacking brain-derived neurotrophic factor develop with sensory deficits. Nature 368(6467):147–150. https://doi.org/10.1038/368147a0
29. Jones KR, Farinas I, Backus C, Reichardt LF (1994) Targeted disruption of the BDNF gene perturbs brain and sensory neuron development but not motor neuron development. Cell 76(6):989–999
30. Korte M, Carroll P, Wolf E, Brem G, Thoenen H, Bonhoeffer T (1995) Hippocampal long-term potentiation is impaired in mice lacking brain-derived neurotrophic factor. Proc Natl Acad Sci U S A 92(19):8856–8860
31. Endres T, Lessmann V (2012) Age-dependent deficits in fear learning in heterozygous BDNF knock-out mice. Learn Mem 19(12):561–570. https://doi.org/10.1101/lm.028068.112
32. Lyons WE, Mamounas LA, Ricaurte GA, Coppola V, Reid SW, Bora SH, Wihler C, Koliatsos VE et al (1999) Brain-derived neurotrophic factor-deficient mice develop aggressiveness and hyperphagia in conjunction with brain serotonergic abnormalities. Proc Natl Acad Sci U S A 96(26):15239–15244
33. Petzold A, Psotta L, Brigadski T, Endres T, Lessmann V (2015) Chronic BDNF deficiency leads to an age-dependent impairment in spatial learning. Neurobiol Learn Mem 120:52–60. https://doi.org/10.1016/j.nlm.2015.02.009
34. Hofer M, Pagliusi SR, Hohn A, Leibrock J, Barde YA (1990) Regional distribution of brain-derived neurotrophic factor mRNA in the adult mouse brain. EMBO J 9(8):2459–2464
35. Murer MG, Yan Q, Raisman-Vozari R (2001) Brain-derived neurotrophic factor in the control human brain, and in Alzheimer's disease and Parkinson's disease. Prog Neurobiol 63(1):71–124
36. Kohara K, Yasuda H, Huang Y, Adachi N, Sohya K, Tsumoto T (2007) A local reduction in cortical GABAergic synapses after a loss of endogenous brain-derived neurotrophic factor, as revealed by single-cell gene knock-out method. J Neurosci 27(27):7234–7244. https://doi.org/10.1523/JNEUROSCI.1943-07.2007
37. Dugich-Djordjevic MM, Peterson C, Isono F, Ohsawa F, Widmer HR, Denton TL, Bennett GL, Hefti F (1995) Immunohistochemical visualization of brain-derived neurotrophic factor in the rat brain. Eur J Neurosci 7(9):1831–1839
38. Oe S, Miki H, Nishimura W, Noda Y (2016) Mechanism of the dendritic translation and localization of brain-derived neurotrophic factor. Cell Struct Funct 41(1):23–31. https://doi.org/10.1247/csf.15015
39. Smith MA, Zhang LX, Lyons WE, Mamounas LA (1997) Anterograde transport of endogenous brain-derived neurotrophic factor in hippocampal mossy fibers. Neuroreport 8(8):1829–1834
40. Dani A, Huang B, Bergan J, Dulac C, Zhuang X (2010) Superresolution imaging of chemical synapses in the brain. Neuron 68(5):843–856. https://doi.org/10.1016/j.neuron.2010.11.021
41. Schoen M, Reichel JM, Demestre M, Putz S, Deshpande D, Proepper C, Liebau S, Schmeisser MJ et al (2015) Super-resolution microscopy reveals presynaptic localization of the ALS/FTD related protein FUS in hippocampal neurons. Front Cell Neurosci 9:496. https://doi.org/10.3389/fncel.2015.00496
42. Danzer SC, McNamara JO (2004) Localization of brain-derived neurotrophic factor to distinct terminals of mossy fiber axons implies regulation of both excitation and feedforward inhibition of CA3 pyramidal cells. J Neurosci 24(50):11346–11355. https://doi.org/10.1523/JNEUROSCI.3846-04.2004
43. Lindvall O, Ernfors P, Bengzon J, Kokaia Z, Smith ML, Siesjo BK, Persson H (1992) Differential regulation of mRNAs for nerve growth factor, brain-derived neurotrophic factor, and neurotrophin 3 in the adult rat brain following cerebral ischemia and hypoglycemic coma. Proc Natl Acad Sci U S A 89(2):648–652
44. Castren E (2014) Neurotrophins and psychiatric disorders. Handb Exp Pharmacol 220:461–479. https://doi.org/10.1007/978-3-642-45106-5_17
45. Lombardi LM, Baker SA, Zoghbi HY (2015) MECP2 disorders: from the clinic to mice and back. J Clin Invest 125(8):2914–2923. https://doi.org/10.1172/JCI78167
46. Tapia-Arancibia L, Aliaga E, Silhol M, Arancibia S (2008) New insights into brain BDNF function in normal aging and Alzheimer disease. Brain Res Rev 59(1):201–220. https://doi.org/10.1016/j.brainresrev.2008.07.007
47. Zuccato C, Cattaneo E (2009) Brain-derived neurotrophic factor in neurodegenerative diseases. Nat Rev Neurol 5(6):311–322. https://doi.org/10.1038/nrneurol.2009.54
48. Li W, Pozzo-Miller L (2014) BDNF deregulation in Rett syndrome. Neuropharmacology 76(Pt C):737–746. https://doi.org/10.1016/j.neuropharm.2013.03.024
49. Sambrook J, Russell, DW. (2001) Molecular Cloning: A Laboratory Manual Cold Spring Harbor Laboratory Press, Cold Spring Harbor
50. Dymecki SM (1996) Flp recombinase promotes site-specific DNA recombination in embryonic stem cells and transgenic mice. Proc Natl Acad Sci U S A 93(12):6191–6196
51. Lessmann V, Heumann R (1998) Modulation of unitary glutamatergic synapses by neurotrophin-4/5 or brain-derived neurotrophic factor in hippocampal microcultures: presynaptic enhancement depends on pre-established paired-pulse facilitation. Neuroscience 86(2):399–413
52. Leschik J, Eckenstaler R, Nieweg K, Lichtenecker P, Brigadski T, Gottmann K, Lessmann V, Lutz B (2013) Embryonic stem cells stably expressing BDNF-GFP exhibit a BDNF-release-dependent enhancement of neuronal differentiation. J Cell Sci 126(Pt 21):5062–5073. https://doi.org/10.1242/jcs.135384
53. Langnaese K, Richter K, Smalla KH, Krauss M, Thomas U, Wolf G, Laube G (2007) Splice-isoform specific immunolocalization of neuronal nitric oxide synthase in mouse and rat brain reveals that the PDZ-complex-building nNOSalpha beta-finger is largely exposed to antibodies. Dev Neurobiol 67(4):422–437. https://doi.org/10.1002/dneu.20317
54. Brigadski T, Lichtenecker, P., Lessmann, V. (2019) Recording activity-dependent release of BDNF from hippocampal neurons.

Neuromethods book Brain-derived neurotrophic factor (BDNF). Edited by Carlos B. Duarte, Enrico Tongiorgi (143)

55. Lessmann V, Dietzel ID (1995) Two kinetically distinct 5-hydroxytryptamine-activated Cl-conductances at Retzius P-cell synapses of the medicinal leech. J Neurosci 15(2):1496–1505
56. Schildt S, Endres T, Lessmann V, Edelmann E (2013) Acute and chronic interference with BDNF/TrkB-signaling impair LTP selectively at mossy fiber synapses in the CA3 region of mouse hippocampus. Neuropharmacology 71:247–254. https://doi.org/10.1016/j.neuropharm.2013.03.041